TTC-2847-R
13 April 1994
Copy No. 14

ThermoTrex Corporation

Atomic Line Filter for SDI Applications

Technial Report for Contract No. N00014-89-C-0068

Prepared for:

Commanding Officer
Guy Beaghler
NCCOSC-RDTE-DIV-804
53570 Silvergate Avenue, Rm. 2070
San Diego, CA 92152-5070

Prepared by:

Jim Menders
ThermoTrex Corporation
9550 Distribution Avenue
San Diego, CA 92121-2305
(619) 578-5885

SECURITY CLASSIFICATION OF THIS PAGE

REPORT DOCUMENTATION PAGE

1a. REPORT SECURITY CLASSIFICATION UNCLASSIFIED	1b. RESTRICTIVE MARKINGS
2a. SECURITY CLASSIFICATION AUTHORITY	3. DISTRIBUTION / AVAILABILITY OF REPORT
2b. DECLASSIFICATION / DOWNGRADING SCHEDULE	
4. PERFORMING ORGANIZATION REPORT NUMBER(S) TTC-2847-R	5. MONITORING ORGANIZATION REPORT NUMBER(S)
6a. NAME OF PERFORMING ORGANIZATION ThermoTrex Corporation 6b. OFFICE SYMBOL (*if applicable*) TTC	7a. NAME OF MONITORING ORGANIZATION Office of Naval Research
6c. ADDRESS (*City, State, and ZIP Code*) 9550 Distribution Avenue San Diego, CA 92123	7b. ADDRESS (*City, State, and ZIP Code*) c/o NCCOSC-RDTE-DIV-804 53570 Silvergate Avenue, Rm. 2070 San Diego, CA 92152-5070
8a. NAME OF FUNDING / SPONSORING ORGANIZATION Strategic Defense Initiative Organization 8b. OFFICE SYMBOL (*if applicable*) SDIO	9. PROCUREMENT INSTRUMENT IDENTIFICATION NUMBER N00014-89-C-0068
8c. ADDRESS (*City, State, and ZIP Code*) 800 North Quincy Street Arlington, VA 22217-5000	10. SOURCE OF FUNDING NUMBERS PROGRAM ELEMENT NO. / PROJECT NO. / TASK NO. / WORK UNIT ACCESSION NO.
11. TITLE (*Include Security Classification*) Atomic Line Filter for SDI Applications	
12. PERSONAL AUTHOR(S) J. Menders, S.H. Bloom, E, Korevaar, M. Rivers, C.S. Liu, P. Searcy, K. Choi	
13a. TYPE OF REPORT Final 13b. TIME COVERED FROM 3/89 TO 9/93	14. DATE OF REPORT (*Year, Month, Day*) 1994 April 13 15. PAGE COUNT 67
16. SUPPLEMENTARY NOTATION	

17. COSATI CODES			18. SUBJECT TERMS (*Continue on reverse if necessary and identify by block number*)
FIELD	GROUP	SUB-GROUP	Atomic line filter, alkali metal vapor, Faraday filter, active optical filter, laser pumped filter, magneto-optic filter, laser communicatons

19. ABSTRACT (*Continue on reverse if necessary and identify by block number*)

When optical signals are embedded in background noise, narrowband optical filters are needed for receivers to achieve quantum limited performance. Such is typically the case with daytime optical communications and lidar. Narrowband filtered detectors, with acceptance bands of just a few picometers (pm) and high out of band rejection are well suited for these applications. The main thrust of this program has been the development of two means for narrowband detection: the Fast Atomic Line Filter/ Field Ion Detector (FALF/FID) and the Faraday magneto-optic filter. The FALF/FIDs transduce optical radiation within a narrow band directly into electrical signals. They are laser pumped filters based on the spectroscopy of atomic vapors. We designed, built and tested an infrared FALF/FID with an rise time of under 10 ns and a quantum efficiency of >25%. Faraday filters are imaging magneto-optic filters with passbands of a few pm. Faraday filters with passbands in the visable and the near infra-red were constructed and tested. Transmission spectra were measured, and found to agree closely with theoretical predictions.

Both of these narrowband detection schemes must be used in conjunction with a tuned narrowband laser source. We developed a frequency locked alexandrite laser designed to match the acceptance band of a rubidium based filter. Finally, a preliminary demonstration of a laser interrogator using a tuned infrared diode laser in conjunction with a filtered receiver was demonstrated.

20. DISTRIBUTION / AVAILABILITY OF ABSTRACT ☒ UNCLASSIFIED/UNLIMITED ☐ SAME AS RPT. ☐ DTIC USERS	21. ABSTRACT SECURITY CLASSIFICATION Unclassified	
22a. NAME OF RESPONSIBLE INDIVIDUAL James H. Menders	22b. TELEPHONE (*Include Area Code*) (619) 578-5885	22c. OFFICE SYMBOL

TABLE OF CONTENTS

*Previously published scientific paper.

ATOMIC LINE FILTER FOR SDI APPLICATIONS

INTRODUCTION

When optical signals are embedded in background noise, narrowband optical filters are needed for receivers to achieve quantum limited performance. Such is typically the case with daytime optical communications and lidar. Narrowband filtered detectors, with acceptance bands of just a few picometers (pm) and high out of band rejection are well suited for these applications. At the start of this program, the narrowband filters that had received the greatest attention were the birefringent and the atomic line (or resonance) filters (ALF). ALFs are a class of filter which use an atomic absorption line provided by an atomic vapor cell to obtain a narrow spectral response to signal photons. In the survey of the state of the art in ALFs by Gelbwachs in Ref. 1, a variety of filters using alkali metal and earth elements were described. The simplest of the filters cited was passive, in contrast to the active filters which required the introduction of optical pumps to activate the filter.

This program investigated two new types of filters, addressed the issue of inrinsic noise common to active ALFs, developed an injection seeded near infrared laser matched to an ALF and demonstrated an atomic line filter application.

NEW FILTERS

We invented a new type of active filter called the Fast Atomic Line Filter/ Field Ion Detector (FALF/FID). The FALF/FIDs transduce optical radiation within a narrow frequency band directly into electrical signals. They are laser pumped filters based on the spectroscopy of atomic vapors. We designed, built and tested an infrared FALF/FID at 780 nm with a rise time of under 10 ns and a quantum efficiency of >25%. We were among the first to recongnize the potential of the Faraday filter for free space laser communications. Faraday filters are imaging magneto-optic filters with passbands of a few pm. Faraday filters with passbands in the visable and the near infra-red were constructed and tested. Transmission spectra were measured, and found to agree closely with theoretical predictions.

INTRINSIC NOISE

"Intrinsic noise" in the context of active ALFs refers to the apparent signal caused by the application of the optical pump needed to activate the filter. The intrinsic noise associated with a filter depends on the vapor spectroscopy and the degree of pumping necessary to activate it. To evaluate the potential of active rubidium and cesium-thallium ALFs, we performed intrinsic noise measurements.

FILTER MATCHED LASER

The narrowband detection schemes we investigated must be used in conjunction with a tuned narrowband laser source. We developed a frequency locked alexandrite laser designed to match the acceptance band of a passive rubidium based filter near 780 nm. The laser featured a electro-optically frequency locked diode laser for use as an injection seeder.

MATCHED OPTICAL TRANSCEIVER

Finally, a preliminary demonstration of components of an optical combat identification system using a Faraday filter were demonstrated. The system was designed to read intensity modulations impressed in a beam retroreflected by an optical responder. The system featured a frequency locked infrared diode laser (852 nm) used in conjunction with a filtered receiver. The interrogator laser frequency locking was accomplished using a Voigt filter (a second magneto-optic atomic line filter related to the Faraday filter) in an optical feedback scheme.

This final report is divided into five sections that collect the main results of this work: (1) Fast Atomic Line Filter, (2) Intrinsic Noise, (3) Faraday Filter, (4) Locked Laser and (5) Combat ID. Sections 1, 3 and 4 contain reprints of scientific papers that describe our results. Section 2 was adapted from an oral presentation originally give by P. Searcy at LASERS '90, San Diego.

REFERENCES

1. Jerry A. Gelbwachs, "Atomic Resonance Filters," IEEE J. Quantum Electron., **24** (7), 1266 (1988).

1. Fast Atomic Line Filter

Fast atomic line filter/field ionization detector

S. H. Bloom, Eric Korevaar, M. Rivers, and C. S. Liu

Thermo Electron Technologies, San Diego, California 92121-2305

Received October 20, 1989; accepted December 26, 1989

An experimental demonstration of a fast atomic line filter/field ionization detector (FALF/FID) is presented. The FALF/FID detects incoming signal photons by resonant absorption in an atomic vapor cell containing a strong electric field. Excited atoms are electric-field ionized after further excitation to a Stark-shifted Rydberg level by a pump laser tuned to a resonance in the ionization spectrum, providing an observed enhancement in the ionization rate of ten times over the continuum ionization threshold. Preliminary measurements of time response (<10 nsec) and quantum efficiency (>25%) indicate that with optimization the FALF/FID will provide high quantum efficiency, fast time response, and narrow-linewidth detection.

Atomic line filters operating at various wavelengths from the near IR to the near UV have been extensively studied, since they are at present the narrowest-bandwidth optical detectors available.[1,2] Their narrow bandwidth and relatively high sensitivity make them extremely useful for detecting weak, narrow-band radiation embedded in a large continuous background. Common to all these filters is internal wavelength conversion by optical atomic transitions and subsequent detection of the converted radiation. In this Letter we describe what is to our knowledge the first experimental demonstration in a vapor cell of a fast atomic line filter/field ionization detector (FALF/FID) that selectively ionizes atoms that have absorbed signal radiation and then detects these ions (or electrons). This filter has the advantages of extremely fast response time and an inherently higher overall quantum efficiency than fluorescence-based filters. (While we were preparing this manuscript, a proposal for such a detector appeared in *Optics Letters*.[3])

The main drawback of using direct photoionization in an atomic line filter is that high pump laser intensities are needed for a fast transition rate to the continuum, which in turn induces intrinsic noise from two-photon ionization. The FALF/FID uses a novel scheme whereby the high pump intensity requirement is alleviated by an order of magnitude by making transitions to semidiscrete Stark-shifted Rydberg levels in an electric field, using the electric field for field ionization and electron/ion collection, a well-studied phenomenon in atomic beams.[4]

For this demonstration we used Rb as the active alkali vapor. Figure 1 shows an abbreviated energy-level diagram for Rb, depicting a schematic representation of the Stark-shifted Rydberg states. The $5p_{3/2}$ state is attained by optical excitation with a diode laser tuned to the atomic transition at 780 nm. After absorption another laser quickly excites the atoms that absorbed the 780-nm photons to Rydberg levels Stark shifted by the application of an external dc field. These levels are of sufficiently high energy that the electric field ionizes them in a time short compared with 1 nsec. The ions/electrons are then detected with near-unity quantum efficiency by an electron multiplier. The field-ionizing level has enough energy classically to ionize in the presence of the electric field, but this ionization is not immediate, and semidiscrete states still exist. Transitions to these states have significantly higher cross sections than transitions to the surrounding continuum. Typical widths of these semidiscrete levels have been measured[5] and depend on the azimuthal quantum number m_l in the direction of the electric field. Widths of $|m_l| = 0$ levels are 1–3 cm^{-1} (1 cm^{-1} = 30 GHz), those of $|m_l| = 1$ are 1–3 GHz, and $|m_l| = 2$ have widths of <100 MHz. (An ionization time constant of ~1 nsec corresponds to a width of ~1 GHz.) For transitions from Rb ($5p$) to the ionization threshold the cross section has been calculated[6] to be $\sim 10^{-17}$ cm^2. For a transition rate of 1/2.5 nsec this requires a pump intensity of 4×10^{25} photons/cm^2 sec, which at 480 nm corresponds to 17 MW/cm^2. The transition cross section to an $n = 20$, $|m_l| = 1$ Stark level can be roughly estimated by assuming a linewidth of 1.5 GHz and an upper-state splitting into 20 levels with $|m_l| = 1$ as

$$\sigma = \frac{1}{20}\frac{A}{8\pi c}\frac{1}{(1/\lambda_{vac})^3}\frac{\omega}{\Delta\omega} \approx 1.4 \times 10^{-16}\ \mathrm{cm}^2, \quad (1)$$

where $A \sim 4.5 \times 10^4$ sec^{-1} for $5p_{3/2} \leftarrow 20d$ transitions. This represents a factor-of-10 improvement over direct ionization. (Similar enhancements are expected

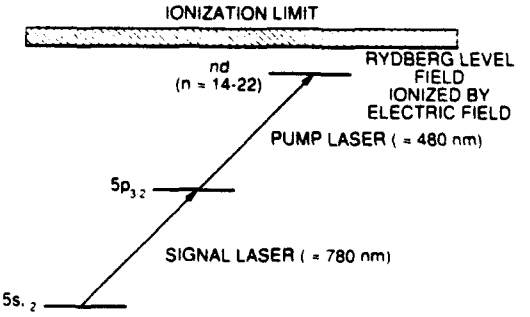

Fig. 1. Energy-level diagram for Rb showing transitions used by the FALF/FID.

0146-9592/90/050294-03$2.00/0

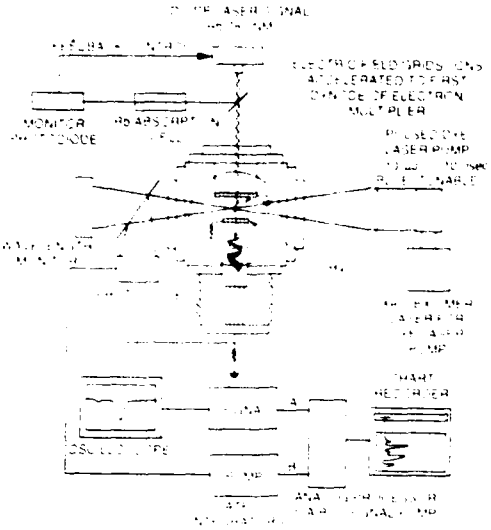

Fig. 2. Experimental setup used to demonstrate the feasibility of the FALF/FID.

for other alkali atoms. For nonalkali atoms the detection scheme might differ.) A laser intensity of ~1.2 MW/cm^2 will be needed for a 2.5-nsec transition time constant. An estimate of the pump laser power in an actual device depends on the active detector area of the device. For Rb, the signal laser at 780 nm has a Doppler-limited absorption cross section of 1.4×10^{-11} cm^2 (including hyperfine structure) so it will be absorbed in an optical depth of 0.01 cm at a density of 6×10^{12} atoms/cm^3, corresponding to a temperature of 105°C and a pressure 3×10^{-4} Torr. If we assume a detector diameter of 0.2 cm, then the pump laser would be focused to a line of 0.01 cm × 0.2 cm with an area of 0.002 cm^2. The necessary laser power is then 2.4 kW, easily attainable with a laser of a few microseconds' pulse length.

An important source of noise that is a function of the atom and of the pump laser's intensity and wavelength is two-photon ionization induced by the pump laser. In Rb at 480 nm the cross section[7] is $\sim 7 \times 10^{-50}$ cm^4 sec. For a pump intensity of 1.2 MW/cm^2 this leads to a transition rate of 0.6/sec. The active volume of the FALF/FID described above contains (6×10^{12} atoms/cm^3) × (0.01 cm × 0.2 cm × 0.2 cm) = 2.4×10^9 atoms. Two-photon ionization for this case will produce only 1.4 electrons/nsec. This intrinsic noise scales with detector area and inversely with the square of the time response. (For direct ionization, requiring 10 times the pump intensity for the same time response, noise levels would be 100 times as high.)

The experimental setup used for measurements of the performance of a Rb FALF/FID is shown in Fig. 2. The interaction region is contained in an evacuated stainless-steel vacuum chamber (7 cm × 7 cm × 7 cm) with sapphire windows. This chamber contains a small amount of Rb metal, which forms an atomic vapor when the chamber is heated. Signal photons at 780 nm (Rb $5s_{1/2} \rightarrow 5p_{3/2}$ transition), produced by an 8-mW, 30-MHz linewidth feedback-controlled diode laser, enter the cell through a reentrant window with an attached electric-field grid and are absorbed in a short distance by the Rb vapor. A second electric-field grid, attached to the electron multiplier, provides both a uniform electric field to the interaction region and an accelerating potential for any ions or electrons produced (depending on the sign of the applied voltage). Tunable (475–492 nm), narrow-band (0.1 cm^{-1}) pump laser light from a 10-μJ, 10-nsec XeCl-laser-pumped grazing-incidence dye laser is focused through the interaction region. Ion (or electron) signals from photoionization of the excited Rb $5p_{3/2}$ atoms are amplified by the electron multiplier and monitored as a function of pump laser wavelength. The output signal, processed with a gated integrator and normalized to the pump laser intensity, is recorded with a strip-chart recorder. The pump laser wavelength is monitored with a high-resolution spectrometer. Although the FALF/FID has a faster time response in the electron collection mode, preliminary data were taken by collecting ions because further refinements, such as light baffles and guard electrodes, are needed to eliminate photoelectrons from scattered pump laser light. In the ion collection mode, two temporally separate signals were seen at the output of the multiplier. A weak signal (factor of 100

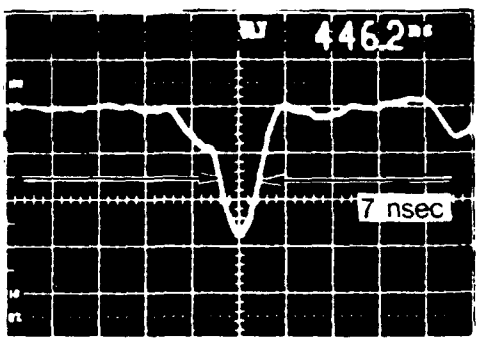

Fig. 3. FALF/FID ion signal showing a time response of ~7 nsec.

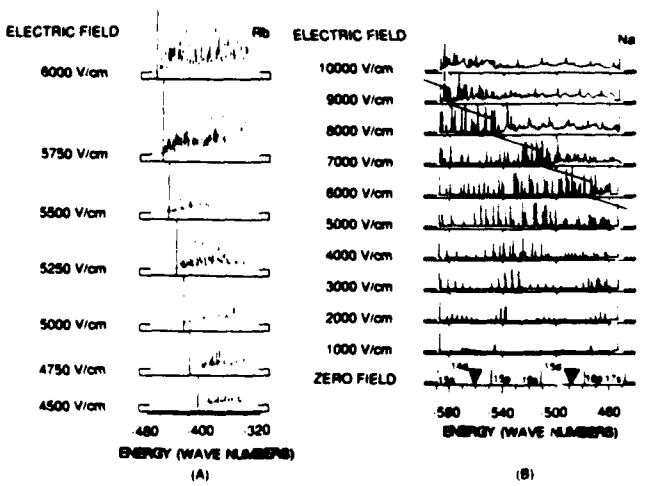

Fig. 4. (A) Field-ionization spectra for Rb taken with the FALF/FID showing the change in the number and size of the various peaks with electric field. (B) Photoexcitation and ionization spectra of a Na atomic beam ($n \approx 15$) in various electric fields.

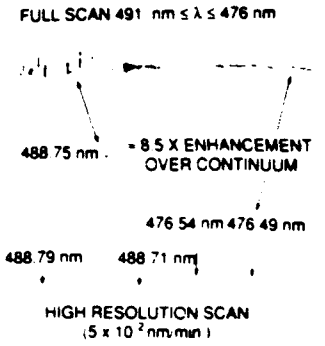

Fig. 5. Field-ionization spectra taken at $E = 6$ kV/cm. The upper spectrum shows the evolution of field-ionized states from semidiscrete resonances to a smooth continuum as the pump laser is varied in wavelength. The lower spectra are high-resolution sections of the upper spectrum, demonstrating approximately a factor-of-8.5 enhancement in ionization cross section for the field-ionized states as opposed to direct ionization.

in size, earlier in time) is due to pump laser light's scattering off the first dynode of the multiplier. A strong ion signal, separated in time from the photoelectric peak by from 20 to 200 nsec, depending on the electric field and the distance of the interaction volume from the electron multiplier field electrode, monitors field ionization. As is shown in Fig. 3, the width of this peak shows a FALF/FID time response of ~7 nsec. When the signal laser is blocked or tuned off the $5s_{1/2}$–$5p_{3/2}$ transition, this peak disappears. Photoexcitation and ionization spectra in the range $n \sim 15$–17 were taken by plotting the field-ionization signal as a function of pump laser wavelength. Some preliminary spectra at different electric fields are shown in Fig. 4(A). The vertical lines represent the classical limit above which field ionization occurs. The spectra show sharp, semidiscrete levels embedded in a broader continuum. For comparison, photoexcitation/field-ionization spectra of Na $3p_{3/2}$ at different electric fields in an atomic beam[9] are shown in Fig. 4(B). By tuning the pump laser to the peaks, large enhancements in the photoionization cross sections are obtained. The abscissa scale was obtained by subtracting the zero-field-ionization limit of ^{85}Rb (33 691.92 cm^{-1}) from the sum of the energy of the $5p_{3/2}$ state (12 816.56 cm^{-1}) and the energy of the blue pump laser. The ordinate scale is arbitrary, although the heights of the spectra are relative to one another. The change in height from high field to low field is due to variations in the dynode voltages of the electron multiplier.

The upper part of Fig. 5 shows a spectrum taken at $E = 6000$ V/cm over a large tuning range of the blue laser. The energy of the pump laser is increasing from left to right in the figure. The spectrum can be seen to go from a series of sharp peaks embedded in a broader-background continuum to a relatively flat, featureless regime above the zero-field-ionization limit. The lower spectra are high-resolution sections of the upper spectrum. The low, broad feature was measured at energies greater than the zero-field-ionization limit ($\lambda_{\text{blue laser}} < 479.05$ nm). The large sharp feature is from the peak near $\lambda_{\text{blue laser}} = 488.75$ nm. The ionization cross section of this Stark-split Rydberg state is enhanced by approximately 8.5 times that of the direct ionization cross section.

A preliminary estimate of the device's quantum efficiency was obtained by reducing the signal laser power to a point at which single-ion events were observed. This led to a calculated quantum efficiency of 28% based on estimates of pump and signal laser overlap volumes. The experimental apparatus is being modified at present to perform a more realistic measurement of the overall quantum conversion efficiency, counting all signal photons entering the apparatus.

In conclusion, the data in Figs. 3–5 demonstrate that a FALF/FID with fast time response and high quantum efficiency can be built. The spectra show that the ionization cross section is significantly enhanced over direct ionization by pumping to Stark-shifted, field-ionized Rydberg states in a strong electric field. A device suitable for lidar applications with a time response of <5 nsec, a quantum efficiency >50%, and an acceptance bandwidth of 0.002 nm should be achievable by using a 1-kW peak-power, long-pulse dye laser as a pump (1 mJ/μsec). Many different operational wavelengths are possible by using different atomic or molecular vapors. In particular, Cs (852 nm), Rb (780 nm), and K (770 nm) match Ti:Al_2O_3, alexandrite, and semiconductor lasers, respectively. Finally, a Cs filter with a 459-nm signal and a 1.06-μm pump can operate in the blue with lower photoelectron and two-photon ionization noise than the IR FALF/FID's.

The research described herein was supported under Strategic Defense Initiative Organization/Innovative Science and Technology/U.S. Office of Naval Research (SDIO/IST/ONR) contract N00014-89-0068. We thank Matt White of SDIO/ONR, Kepi Wu of SDIO, and Vern Smiley and Guy Beaghler of ONR for their encouragement and support.

References

1. For a thorough review, see J. A. Gelbwachs, IEEE J. Quantum Electron. **24**, 1266 (1988).
2. E. Korevaar, M. Rivers, and C. S. Liu, Proc. Soc. Photo-Opt. Instrum. Eng. **1059**, 111 (1989).
3. T. Okada, H. Andou, Y. Moriyama, and M. Maeda, Opt. Lett. **14**, 987 (1989).
4. D. Kleppner, M. G. Littman, and M. Zimmerman, in *Rydberg States of Atoms and Molecules*, R. F. Stebbings and F. B. Dunning, eds. (Cambridge U. Press, Cambridge, 1983).
5. J. Y. Liu, P. McNicholl, D. A. Harmin, T. Bergeman, and H. J. Metcalf, in *Atomic Excitation and Recombination in External Fields*, M. H. Nayfeh and C. W. Clark, eds. (Gordon & Breach, New York, 1985).
6. M. Aymar, O. Robaux, and S. Wane, J. Phys. B **17**, 993 (1984).
7. H. Bebb, Phys. Rev. **149**, 25 (1966).
8. M. G. Littman and H. J. Metcalf, Appl. Opt. **17**, 2224 (1978).
9. E. Korevaar, Ph.D. dissertation (Princeton University, Princeton, N.J., 1987).

A BLUE-GREEN FAST ATOMIC LINE FILTER/FIELD IONIZATION DETECTOR

ABSTRACT

A modification of a previously experimentally demonstrated infra-red (IR) fast atomic line filter/ field ionization detector (FALF/FID) is presented. The modification changes the signal wavelength from IR to blue-green (455 or 459 nm). The FALF/FID detects incoming signal photons by resonant absorption in an atomic vapor cell containing a strong electric field. Excited atoms are electric field ionized after further excitation to a Stark shifted Rydberg level by a pump laser tuned to a resonance in the ionization spectrum, providing an observed enhancement in the ionization rate of ten times over the continuum ionization threshold. We describe the operation of the blue cesium FALF/FID and our progress towards a feasibility demonstration.

1. INTRODUCTION

Atomic line filters operating at various wavelengths from the near IR to the near UV have been extensively studied since they are presently the narrowest bandwidth optical detectors available[1,2]. Their narrow bandwidth and relatively high sensitivity make them extremely useful for detecting weak narrowband radiation such as a laser signal embedded in a large continuous background. This makes them useful in applications such as LIDAR, underwater detection, and satellite tracking for example. Common to all of these filters is internal wavelength conversion via optical atomic transitions and subsequent detection of the converted radiation. In this paper we propose a modification of a previously experimentally demonstrated[3] (using rubidium as the active vapor, 780 nm signal) Fast Atomic Line Filter/Field Ionization Detector (FALF/FID) that selectively ionizes atoms that have absorbed signal radiation and then detects these ions (or electrons). This filter has the advantages of extremely fast response time, and since the ions/electrons can be detected

with near unity quantum efficiency, it has an inherently higher overall quantum efficiency than fluorescence based filters.

The main drawback of using direct photoionization in an atomic line filter is that high pump laser intensities are needed for a fast transition rate to the continuum which in turn induces intrinsic noise due to two photon ionization. The FALF/FID uses a novel scheme whereby the high pump intensity requirement is alleviated by an order of magnitude by making transitions to semi-discrete Stark shifted Rydberg levels in an electric field, using the electric field for field ionization and electron/ion collection, a well studied phenomenon in atomic beams[4].

The fast time response and high quantum efficiency of this filter make it very useful for underwater detection applications. The filter time response of < 5 nsec allows the illuminator pulse to be short, also < 5 nsec which gives good depth resolution (on the order of 3 x 10^8 m/sec*5 nsec = 1.5 meters). The operating wavelengths of either 455 or 459 nm have the advantage of optimal deep water transmission. The high quantum efficiency allows detection of the very low return signal levels, usually a few hundred photons, typical of underwater objects illuminated with available laser powers at either 455 or 459 nm. In addition, the small acceptance bandwidth (< 0.002 nm) gives the FALF/FID the high background rejection necessary to detect these signals. The filter is also easily gateable which allows for the rejection of unwanted return scatter from the illuminator. The illuminating laser for 459 nm already exists (lead Raman shifted XeCl or dye lasers) and the illuminator for 455 nm could be the same lasers currently being developed for submarine laser communications programs. Finally, the pump laser could be a modest solid state laser, either Nd:YAG at 1.064 μ or Nd:BEL at 1.079 or 1.070 μ operating at a few tens of millijoules energy and a few hundred nanoseconds pulselength. The required pump power could be reduced even further if the pump beam were to be reflected in a multipass geometry. This allows for the possibility of a very compact system that uses only one laser source. A fraction of a Nd:BEL beam can be frequency doubled and used to pump a Ti:Sapphire crystal which, using sum frequency generation with another fraction of the Nd:BEL beam, is converted to 455 nm producing the illuminator light while the remaining fraction of the Nd:BEL beam can be used to pump the FALF/FID.

2. OPERATING PRINCIPLE

For the proposed blue FALF/FID demonstration we will use cesium (Cs) as the active alkali vapor. In principle one could choose to have the signal laser tuned to the $6s_{1/2}$-$7p_{3/2}$ transition at 455.52 nm or the $6s_{1/2}$-$7p_{1/2}$ transition at 459.31 nm. For the proof of principle experiment we will use the 459.31 nm transition since a signal laser at this wavelength already exists (Pb Raman shifted XeCl) and for detecting this wavelength the filter's pump can be a Nd:YAG laser operating at 1.064 μ. Figure 1 shows an abbreviated energy level diagram for Cs, depicting a schematic representation of the Stark-shifted Rydberg states. The $7p_{1/2}$ state is attained by optical excitation with a laser tuned to the atomic transition at 459.31 nm. After absorption another laser quickly excites the atoms that absorbed the 459.31 nm photons to Rydberg levels Stark shifted by the application of an external D.C. field. For a Nd:YAG pump laser, these levels correspond to n ~ 26. The threshold field necessary for field ionization of this level is about E= 700 V/cm, which should be easily attainable at the contemplated operating temperature. These levels are of sufficiently high energy that the electric field ionizes them in a time short compared to 1 ns. The ions/electrons are then detected with near unity quantum efficiency by an electron multiplier. The field ionizing level has enough energy classically to ionize in the presence of the electric field, but this ionization is not immediate and semi discrete states still exist. Transitions to these states have significantly higher cross sections than transitions to the surrounding continuum. Typical widths of these semi-discrete levels have been measured[5] and depend on the azimuthal quantum number m_l in the direction of the electric field. Widths of $|m_l| = 0$ levels are 1-3 cm^{-1} (1 cm^{-1} = 30 GHz), $|m_l| = 1$ are 1-3 GHz and $|m_l| = 2$ have widths < 100 MHz. [An ionization time constant of ~1 ns corresponds to a width of ~1 GHz].

3. PUMP LASER POWER REQUIREMENT

Cross section data for transitions from Cs (7p) to the ionization threshold are not presently available. The cross section for Cs(6p) to the ionization threshold[6] has been calculated to be about 10^{-18} cm^2. For a transition rate of 1/5 ns this requires a pump

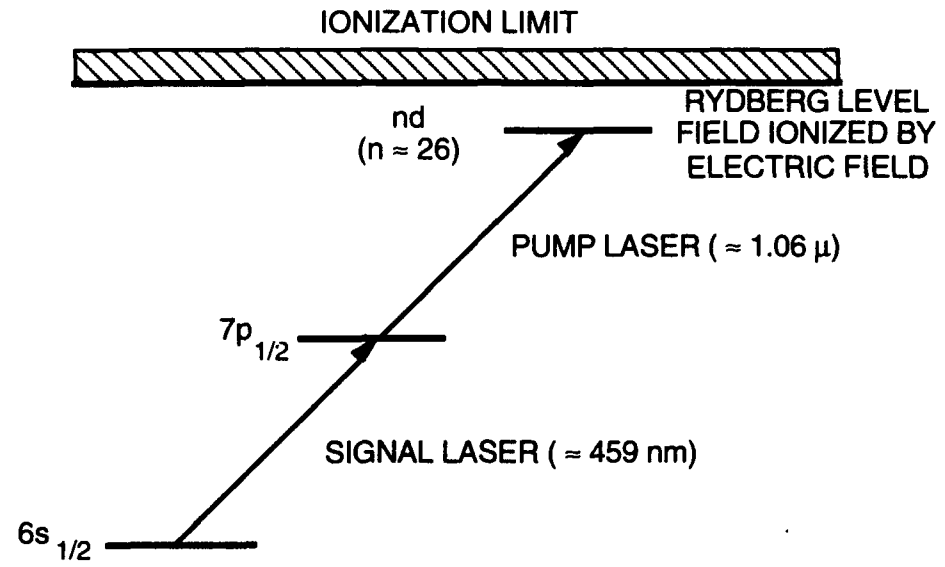

90-11643

Figure 1. Energy level diagram for cesium showing transitions used by the FALF/FID.

intensity of 2 x 10^{26} photons/cm2 sec which at 1.064 microns corresponds to 37 MW/cm^2. The transition cross section to an n = 26, $|m_l|=1$ Stark level can be roughly estimated by assuming a linewidth of 1.5 GHz and an upper state splitting into 26 levels with $|m_l|=1$ as:

$$\sigma = \frac{1}{26} \times \frac{A}{8\pi c} \times \frac{1}{(1/\lambda_{vac})^3} \times \frac{\omega}{\Delta\omega} \approx 7.4 \times 10^{-17}\ \text{cm}^2 \qquad (1)$$

where A ~ 6.42 x 10^3 sec^{-1} for $7p_{1/2} \leftarrow$ 26d transitions[7]. This represents a significant improvement over direct ionization. Figure 2 shows the pump laser intensity necessary for a given time response. A laser intensity of about 500 kW/cm^2 will be needed for a 5 ns transition time constant. An estimate of the pump laser power in an actual device depends on the active detector area of the device. For cesium, the signal laser at 459 nm has a Doppler limited absorption cross section of 2.6 x 10^{-14} cm^2 so it will be absorbed in an optical depth of 0.5 cm at a density of 7.7 x 10^{13} atoms/cm^3 corresponding to a temperature of 129°C and a pressure 3 x 10^{-3} torr. If we assume a detector diameter of 0.2

cm, then the pump laser would be focussed to a line of 0.5 x 0.2 cm with an area of 0.1 cm^2. The necessary laser power is then 50 kW, easily attainable with a 15 mJ, 300 ns laser.

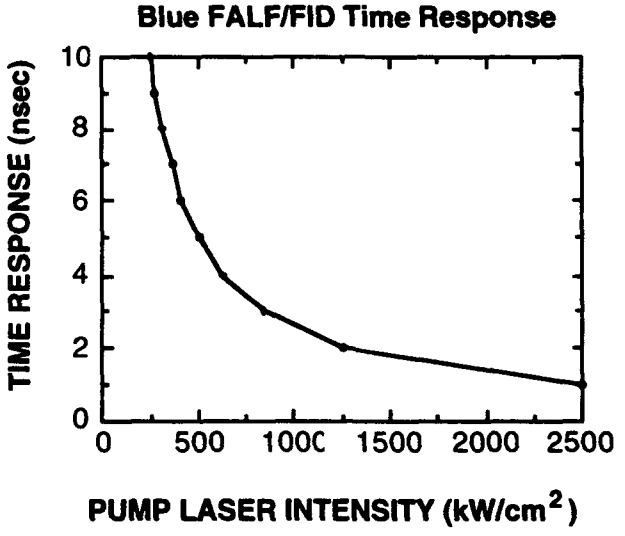

Figure 2. Pump laser intensities necessary for direct and field ionization for a given time response. Also plotted is the four photon ionization noise associated with a given pump intensity.

At an operating temperature of 129°C the pressure is about 3 x 10^{-3} torr and the electron mean free path is about 1 meter, much larger than the size of the device, so it should not suffer any collisions en route to the detector. For a cell size of 0.5 cm and a 1 kV/cm electric field the electron transit time is less than 1 ns, which will have a negligible effect on the speed of the device.

4. NOISE

Calculations of four photon[8], thermionic, thermal ionization and photoelectron noise show that the contribution from each of these possible noise sources is negligible.

Four photon noise produces less than 5.5×10^{-8} electrons/ns at a 500 kW/cm^2 pump intensity. The noise contribution from thermionic emission is given by the Richardson-Dushman equation. For our case Cs has a work function of 1.81 eV which gives a noise contribution at 129 °C of $< 3 \times 10^{-6}$ electrons/cm2 ns, which is negligible. The Boltzmann factor to the $7p_{1/2}$ state is $<1 \times 10^{-31}$ so thermal ionization is not important. Finally, the energy of photons at 1.064 μ is 1.165 eV, which is less than the work function of cesium and therefore scattered pump light producing photoelectrons should not be a problem.

A possible important source of noise could be electrical breakdown due to the high voltage applied to the accelerating grids and the electron multiplier. Data for low pressure nitrogen breakdown[9] show that the Paschen curve minimum occurs at an electrode spacing/pressure product of about 10^{-3} atm-cm. For a 1 cm electrode spacing, typical for the FALF/FID, the breakdown voltage is about 10^4 volts at 3×10^{-3} torr, or 10^4 volts/cm. The blue FALF/FID only needs to hold off about 10^3 volts/cm which should be achievable. If cesium vapor breaks down at significantly lower voltages it might be necessary to operate the filter at lower temperature which would require increasing the pump power to maintain the same efficiency.

5. FEASIBILITY DEMONSTRATION PROGRESS

The most important characteristic of the FALF/FID for LIDAR applications is its high quantum efficiency. In order to measure the quantum efficiency of the device accurately, the electrode geometry must be designed carefully. The following is a list of the important parameters for determining the quantum efficiency with accuracy:

1) The signal absorption volume must be known accurately. In order to do this, the entrance window for the signal beam must either have the electrode coated on its surface, or have an extremely fine wire mesh in close contact with it. Experiments performed in Phase I with rubidium as the atomic vapor showed that using an Inconel film of thickness such that it had an optical density of 0.5 as the electrode was unsatisfactory. The film "etched" such that it was non-uniform in optical density over its surface after a few hours of testing. The etching seemed to be due to electrons from the field ionization process (we were collecting ions in that experiment) which were accelerated back towards the entrance

window electrode (due to the bias arrangement used for collecting ions). The "grid" electrode in that experiment was constructed from a coarse stainless steel wire mesh the pattern of which transferred back to the entrance electrode, indicating that the etching was not due to a chemical reaction with the alkali vapor, but a milling process by charged particles following the electric field lines back to the entrance window electrode. Therefore one must use a macroscopic mesh as the entrance signal electrode. Since the absorption depth for operating the cesium in the IR mode is about 100 μ, the screen must be kept thinner than this and in addition it must make intimate contact with the window over the entire signal beam diameter.

2) The pump laser beam must be spatially profiled.

3) The signal strength vs. pump laser power should be saturated at the pump laser power used to make the measurement. This ensures that all of the excited atoms are field ionized

4) Collection of the ions or electrons must be apertured to the signal beam diameter. Since the pump laser could cause multiphoton ionization noise, one should only collect ions or electrons from the active volume to exclude ions or electrons produced by the pump laser alone.

The electrode used to solve step one was made from 25 μ stainless steel mesh which had a 30% shadowing factor. The total thickness of the mesh was 50 μ at most (at the points where two wires crossed) and the openings in the mesh were 25 μ maximum. Therefore at a distance of about 2-3 times the radius of the hole (12 μ x 2 = 25 μ) the electric field is uniform and behaves as if the mesh were a continuous electrode. In order to assure that the screen contacted the window over the signal beam diameter, the window was made with a slight curvature. This insured that at least one point of the screen was snug against the window , and in fact if the beam diameter was made small enough (< 2 mm)this insured that we could determine exactly how many signal photons reached the active volume. Figure 3 shows a plot of the equipotentials for our electrode geometry, which allows calculation of the active volume electric field and in addition shows that the electric field over the active volume is uniform. Finally, the grid electrodes a solid stainless steel plate with a 2 mm aperture in the center. This permits collection of ions or electrons

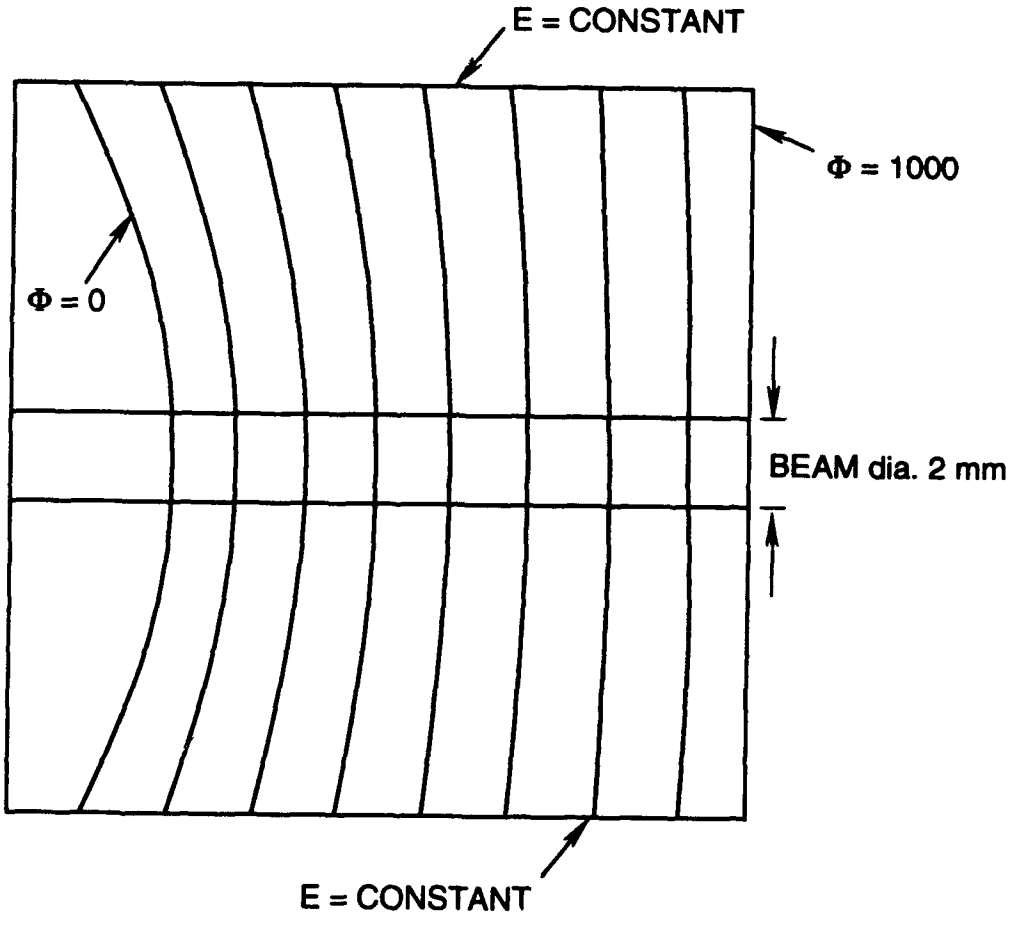

Figure 3. Equipotentials for the FALF/FIP electrode geometry.

from the active region only, and excluding any ions or electrons produced by the pump laser alone.

Figure 4 shows the geometry of the initial lab model. The device consisted of a Thorn EMI electron multiplier encased in a glass envelope containing cesium metal. The device is self contained (no vacuum system necessary) and portable. Unfortunately this model did not work. The electron multiplier is supplied with the dynode biasing resistors inside of the tube. Upon initial heating of the cell the cesium vapor attacked and destroyed the resistors. The tube was then modified by replacing the ruined resistors with glass encapsulated hermetically sealed resistors. Again the tube failed upon heating, except the failure mode was electrical breakdown of an unknown gas inside of the device. The resistors are sealed in argon and it is possible that one or more of them leaked. The resulting low pressure of argon is quite easily broken down by the fields used in the FALF/FID.

Rather than rework the same device, it was decided to replace the multiplier with one that had the individual dynode wires exiting the glass envelope and therefore could be biased externally. Another device was constructed using a Thorn PMT that had its photocathode removed so it essentially functioned as an electron multiplier. This device could be biased to high voltage (6kV/cm) without causing internal breakdown.

Figure 5 shows output of a cesium reference cell photodiode and the output of the FALF/FID at 100 °C which corresponds to a cesium density of $10^{13}/cm^3$. The signal laser is being ramped in wavelength through the two cesium hyperfine peaks at 852 nm(about 9 GHz apart). The top trace from the reference cell shows the absorption at each peak and the lower trace shows the ion signal form the FALF/FID. This ion signal is not due to field ionization of Stark-shifted Rydberg states but is due to ionization caused by tight focussing the 852 nm signal laser into the cell alone. The ion signal is due to collisional ionization of cesium excited state atoms.

The next step would have been to use a pump laser at 520 nm to excite the excited cesium atoms to a Rydberg state and then field ionize them. Unfortunately the cell did not last long enough to perform this measurement. The cesium reacted with the glass used to electrically insulate the high voltage leads exiting the cell. This reaction reduced the resistance of the glass feedthrough to a near short and therefore the multiplier could no

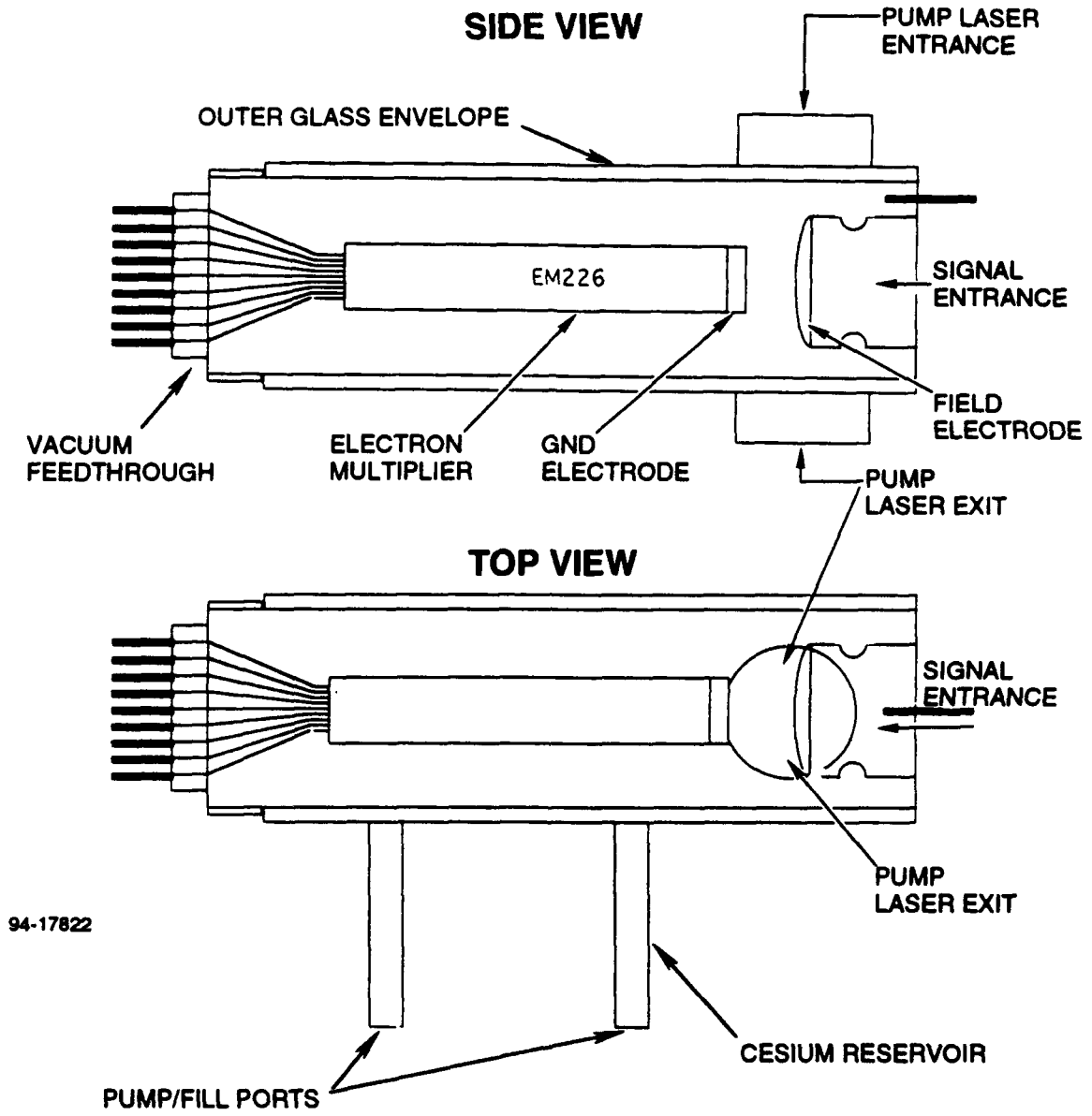

Figure 4. Geometry of initial lab model.

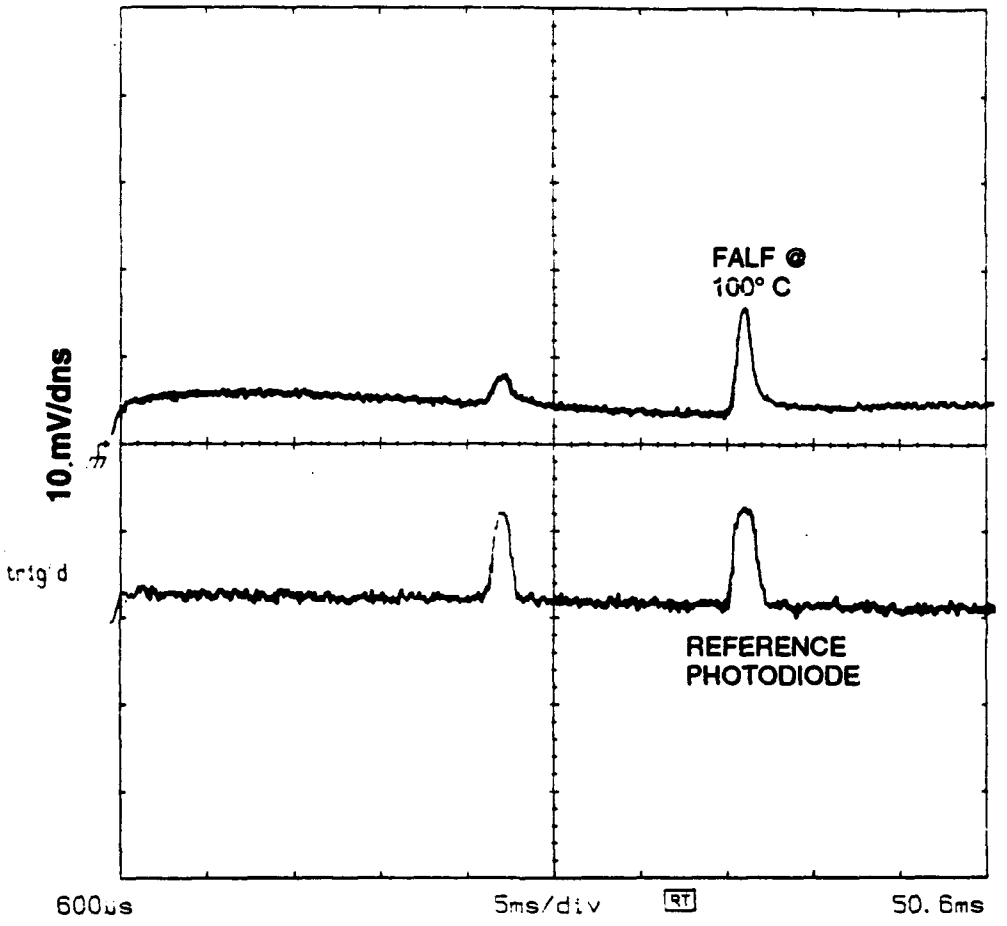

94-17820

Figure 5. Output of a cesium cell reference photodiode and FALF/FIP at 100° C.

longer be biased properly which of course reduced the multiplier gain to a point where a signal was no longer visible.

It turns out that cesium and for that case all alkali metals react with SiO_2. Much literature is available on so called thermionic diodes which mainly used cesium as the active element at very high temperature. From these studies it was concluded that cesium reacts badly with SiO_2 and glass should not be used as an electrical insulator if it comes in contact with cesium vapor. These same reports also mention that high purity alumina does not react with cesium and was used successfully in many thermionic diode systems as an electrical insulator.

Figure 6 shows the final version of the FALF/FID which is presently under construction. The glass-metal electrical feedthroughs have been replaced by alumina-metal feedthroughs. The multiplier is the same one used earlier except all of the glass has been removed. The only materials remaining inside of the device that could contact the cesium vapor are Be-Cu (dynodes), stainless steel, and high purity alumina, none of which react with cesium. The entire device is housed in a glass envelope whose only purpose is to maintain the cesium atmosphere, it does not hold off any voltage.

6. CONCLUSIONS AND RECOMMENDATIONS

The proof of principle experiment in phase one showed that the FALF/FID concept is valid. There is no physical reason why the same concept should not work in cesium. Engineering the FALF/FID will take more work due the materials problems associated with alkali metal vapors. We believe that the last modification of the FALF/FID will alleviate the problems seen in the earlier versions. The quantum efficiency measurement will be performed assuming the FALF/FID cell is viable.

If this last modification does not work for some unforeseen reason there is still another idea that might solve the problem of alkali reactivity. Recently thin films of CVD diamond have become commercially available and in particular one can purchase a 0.4μ thick x 6 mm diameter diamond film that will withstand a one atmosphere pressure differential. Electrons of energy 10 keV or greater can easily penetrate such a film. This film could be used at the entrance of the multiplier to keep the dynodes under high vacuum and keep the cesium vapor away from the dynodes. The cell can be designed (see figure 7)

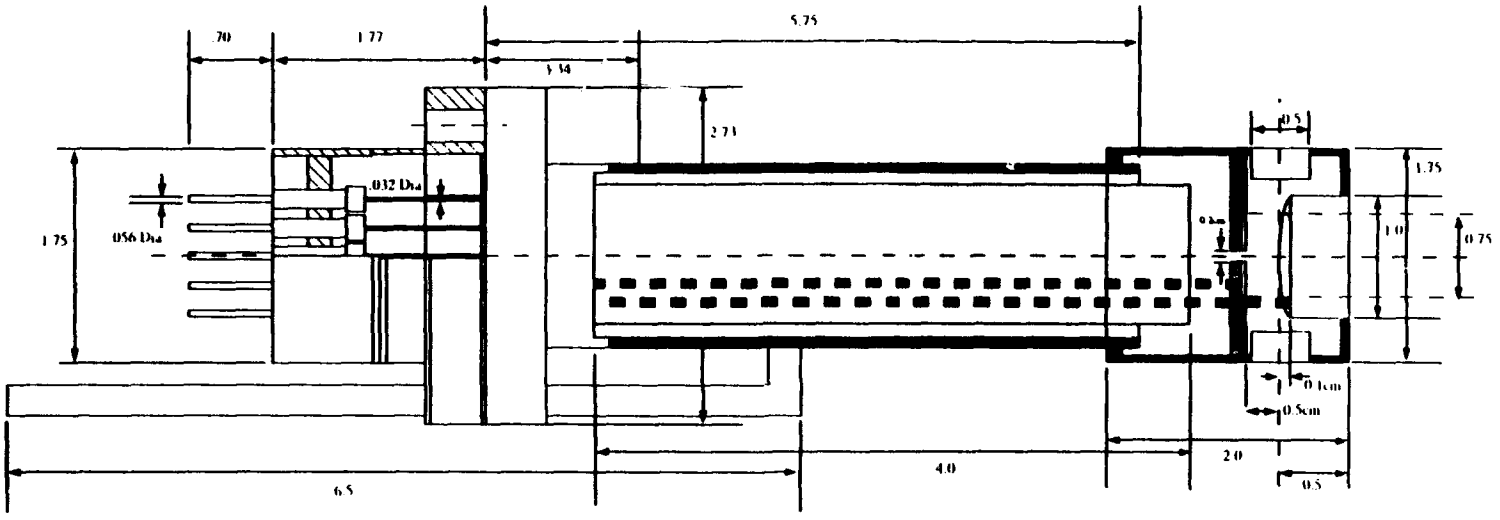

94-17819

Figure 6. Final version of FALF/FIP currently under construction.

such that the cesium vapor is contained in a cell that does not have any high voltage leads from the dynodes passing through it. The only foreseeable problem that could arise is breakdown of the cesium vapor at this voltage although preliminary experiments performed here suggest that this is not a problem. This could be the best solution to the long term materials problems associated with alkali vapors and high voltage feedthroughs.

7. REFERENCES

1. For a thorough review, see J. A. Gelbwachs, IEEE J.Q.E., **QE-24**, 1266 (1988).

2. E. Korevaar, M. Rivers, C.S. Liu, SPIE Proceedings, **Vol. 1059**, 111, (1989).

3. S.H. Bloom, Eric Korevaar, Mike Rivers, and C.S. Liu, to appear in March 1, 1990 issue of Optics Letters.

4. D. Kleppner, M.G. Littman, M. Zimmerman, *Rydberg States of Atoms and Molecules*, R.F. Stebbings and F.B.Dunning eds. (Cambridge Univ. Press, 1983).

5. J.Y. Liu et. al. *Atomic Excitation and Recombination in External Fields*, M.H. Nayfeh and C.W. Clark eds. (Gordon and Breach, NY, 1985).

6. Y. V. Moskvin, Opt. Spectrosc. **15**, 316-318, (1963).

7. Extrapolated from data in: A. Lindgard, and S.E. Nielsen, "Transition Probabilities for the Alkali Isoelectronic Sequences Li, Na, K ,Rb ,Cs ,Fr," in *Atomic Data and Nuclear Data Tables* **19**, 533-633 (1977).

8. D. Normand and J. Morellec, J. Phys. B.,**13**, 1551-1561 (1980).

9. T. J. Gallagher and A.J. Pearmain, in *High Voltage- Measurement, Testing and Design*, John Wiley and Sons, Chichester (1983).

10. E. Korevaar, PhD Thesis, Princeton Univ., Dept. of Aero. and Mech. Eng. (1987) p. 98.

2. Intrinsic Noise

ACTIVE ATOMIC LINE FILTER INTRINSIC NOISE MEASUREMENTS

Paul Searcy, Kyunam Choi, Scott Bloom, Eric Korevaar and C.S. Liu

ABSTRACT

We investigated the amount of in-band optical noise and the production mechanisms in two active atomic line filters, rubidium and cesium-thallium. We conclude from our experiments that actively pumped atomic line filters in rubidium and cesium that rely on the creation of an excited population by pumping from the ground state show significant intrinsic noise fluorescence. The noise is due primarily to collisional excitation of high lying levels including collisional ionization.

Actively pumped atomic line filters have been proposed for use in a system matching doubled neodymium lasers for Submarine Laser Communications (SLC). In particular, the most promising filter concepts are the cesium-thallium[1] filter for receiving signal light at 535 nm (matching doubled Nd:BEL) and rubidium[2] at 532 nm (matching doubled Nd:YAG). These filters consist of a green pass filter, an alkali vapor cell, and an ultraviolet pass filter. As shown in Figure 1, pump photons excite the alkali atoms from the ground state, creating a population of excited alkali atoms. The green signal photons from the transmitter are passed through a broadband colored glass filter and are matched to an upper state transition in the vapor allowing excitation to an even higher level. As this level decays back to the ground state the atom emits blue and UV secondary signal photons which pass through a second colored glass filter and are detected by a PMT. Background light is blocked by the two colored filters allowing only upconverted light to pass through the filter. Unfortunately, UV photons can also be generated by the pump laser alone by various mechanisms, with no signal photons present, resulting in intrinsic noise. Other filter schemes which use a local IR pump laser to pump from a non-ground state level do not create noise photons and remain viable concepts for use with IR systems.[3,4] Our task was to determine if these noise photons would interfere with operation of the SLC-type system, and what those noise generation mechanisms were.

The severity of the noise generation in the rubidium filter is obvious when a cell of rubidium is pumped by a Ti:Sapphire laser at the intensity required by an active filter. The laser was tuned to the 780 nm resonance creating blue fluorescence clearly visible to the human eye in an illuminated room as shown in Figure 2. A Schott colored glass filter (BG 39), similar to the second colored glass filter in an atomic line filter, was placed in front of the left side of the cell blocking all wavelengths except those between 300 and 700 nm. We realized that these photons would appear in the signal channel along with the secondary signal photons generated at 323, 335, 359 and 421 nm by a green laser signal at 532 nm. In fact, when the fluorescence was imaged through a scanning monochromator the noise was discovered to fall on precisely those secondary signal wavelengths which eliminates any chance of using narrower-band interference filters instead of colored glass filters. As seen in Figure 3 the dominant noise peaks were observed at 421 and 359 nm while the more UV transitions at 335 and 323 nm were too small to be detected on the same scale. In

theory, it would be possible to block the 421 and 359 nm noise sources and use the 335/323 nm transitions in the ALF system. Unfortunately the branching ratios from the 9p state in rubidium are much smaller for the UV transitions (part of the reason the noise is smaller) so the quantum efficiency of the filter would suffer.

Similar investigations of the cesium-thallium filter with the scanning monochromator and pumping laser at 852 nm gives similar results as shown in Figure 4. Noise signals from 7p, 8p, and 9p to 6s transitions are identical in wavelength to the secondary signal photons generated in the proposed filter operation.

We believe the noise was generated by two main mechanisms, multiphoton excitation and collisional excitation as shown in Figure 5. In multiphoton excitation, photons from the pump laser create an excited state population at the 6p level which can be further excited to the 7p level and beyond the ionization limit. One pathway to the 7d state is through a Raman transition enhanced by the nearby 6d level. Collisions between atoms at the 6p level can create multiply excited cesium atoms: for example a binary collision $Cs^* + Cs^*$ can result in doubly excited Cs^{**}. The decay of multiply excited cesium atoms (Cs^{n*}) results in ultraviolet noise photons.

The details of the multiphoton and collisional noise processes are given by the reactions in Figure 6. We could distinguish between multi-photon and collisional excitations by their interaction bandwidths from the 6p state. The interaction bandwidth can be investigated in a pump-probe experiment where the pump laser is tuned to the 852 nm ground state-6p transition and the probe laser scanned over the same transition. Comparing the multi-photon and collisional mechanisms shows the important difference in the sensitivity of noise generation to probe laser detuning. We expect the multiphoton process from the 6p state to give a relatively broad and asymmetric noise spectrum due to its insensitivity to probe laser detuning. We performed the simple experiment shown in Figure 7 where one diode laser (the pump laser) is locked to one of the peaks of the hyperfine doublet near 852 nm generating a constant level of 455 nm noise as shown in the oscillogram labeled "pump laser only." A second diode laser (the probe) was aligned to pass through the same volume and was tuned through the hyperfine doublet. The probe laser alone produced the noise

signal shown in the oscillogram labeled "probe laser only." Evidence for the collisional mechanism rather than the multiphoton excitation mechanism is demonstrated in the sharpness of the peaks in Figure 7. The oscillogram labeled "both lasers" demonstrates the expected strong resonant dependence and gives no indication of the broad and asymmetric noise spectra expected from multiphoton excitation. With both beams pumping the same volume (doubling the pump intensity) more than a doubling of the noise is observed on the oscillogram labeled "both lasers." This demonstrates the quadratic or cubic dependence the noise level has versus pumping power. Further experiments to quantify the actual exponent value n (as used in Figure 6) gave values between n = 2 and n = 3, implying that both two and three collisions are occurring in the generation of the 455 nm noise peak.

We conclude from our experiments that actively pumped atomic line filters that rely on the creation of an excited population in rubidium and cesium by pumping from the ground state show significant intrinsic noise fluorescence. This level of noise indicates the filters are not appropriate for most traditional ultra-narrow band applications. The noise is due primarily to collisional excitation of high lying levels including collisional ionization and is unavoidable since high levels of pumping are required to create a sufficiently dense population of excited atoms to absorb incoming green signal photons.

References

1. Liu, Chantry, Chen, SPIE Proc. 709, 132-138 (1986).
2. Shay, Chung, Optics letters 13, 443 (1988).
3. Korevaar, Rivers, Liu, SPIE Proc. 1059. 111-118 (1989).
4. J. A. Gelbwachs, "Atomic Resonance Filters," IEEE J. Quantum Electronics 24, 1266-1277, 1988.

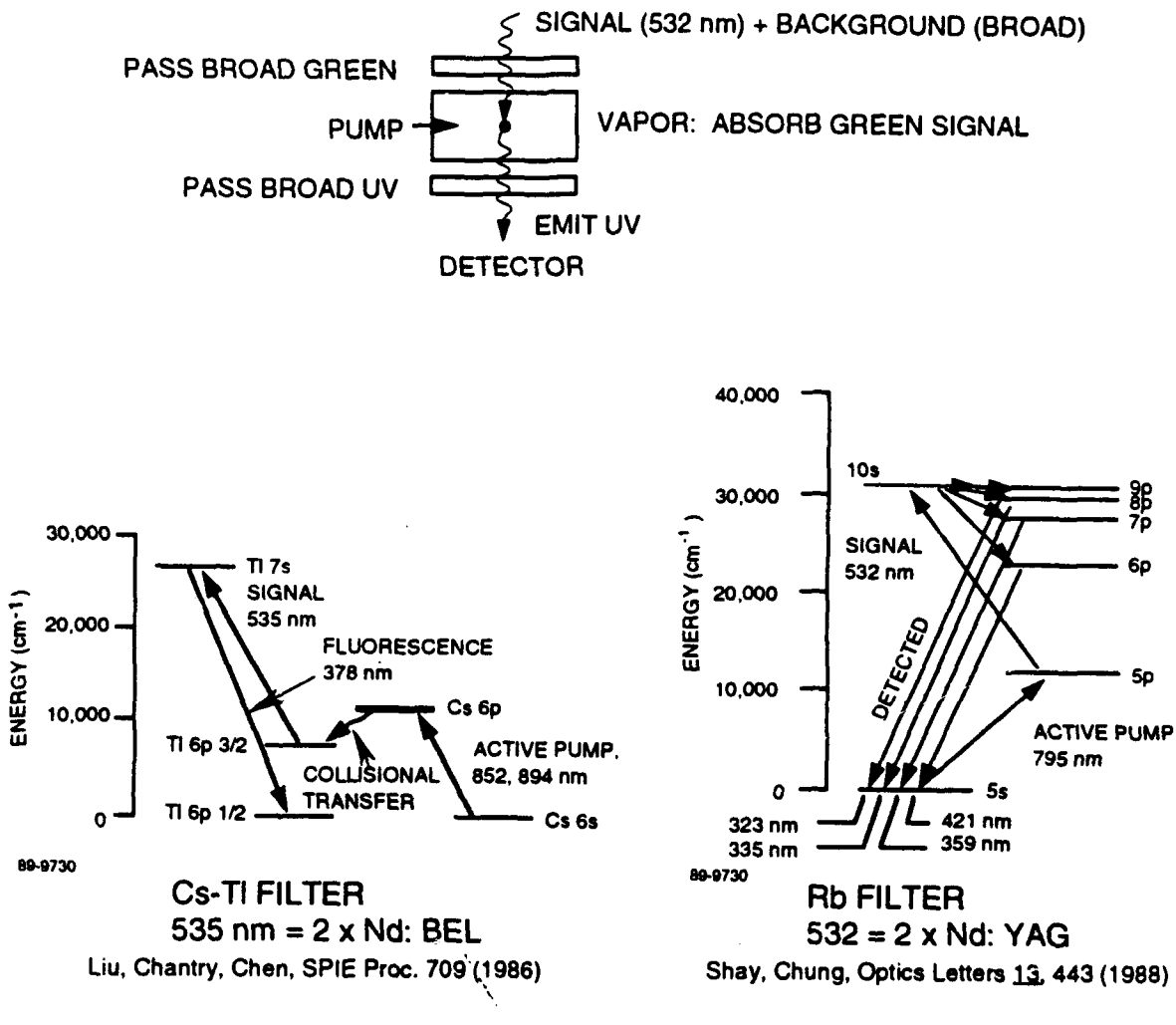

90-13055

Figure 1. Cs-T ℓ filter and active Rb filters.

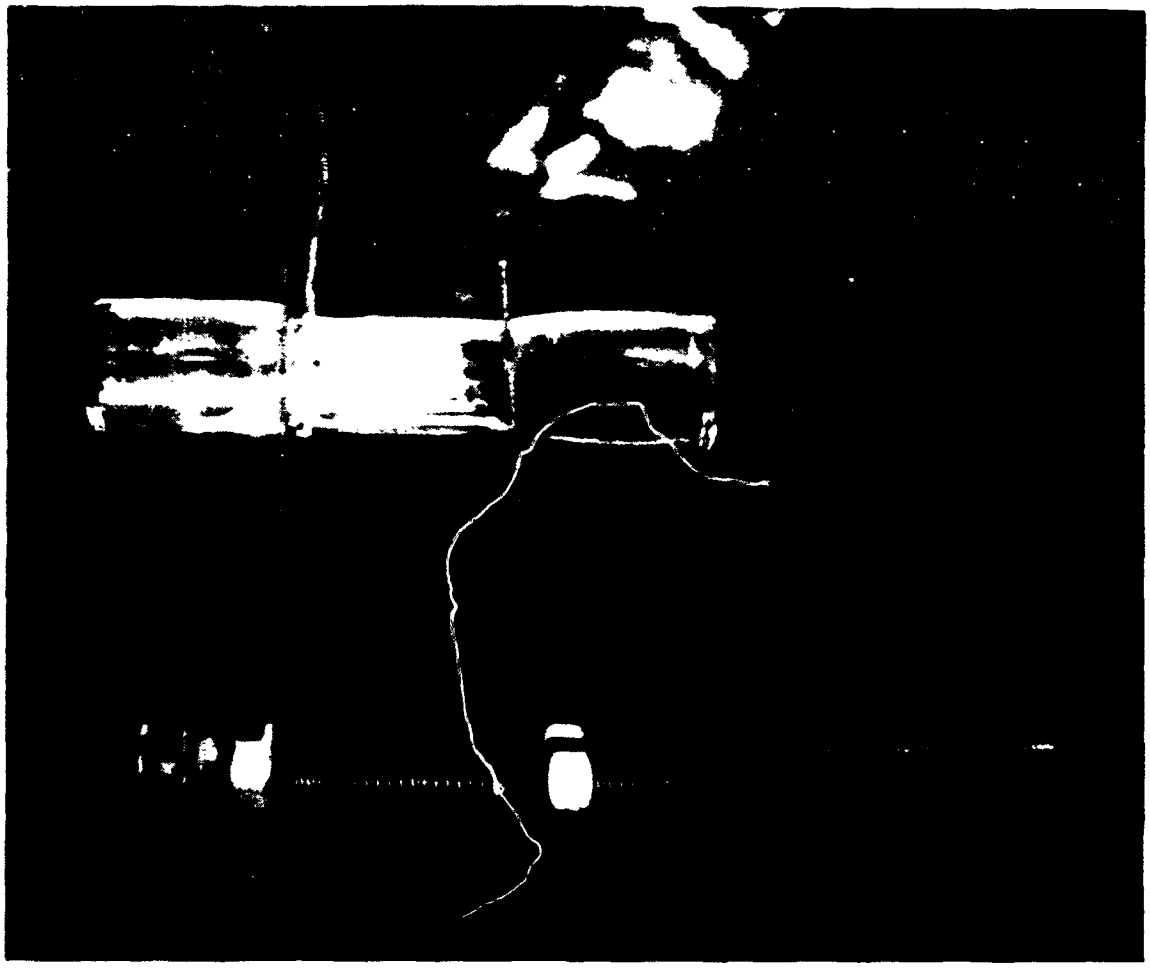

Ti: Al_2O_3 PUMP, λ =780 nm
BEAM POWER $\cong$ 100 mW; AREA $\cong$ 0.1 cm^2 ; INTENSITY $\cong$ 1 W/cm^2 ;
LINEWIDTH $\cong$ 10 GHz; VAPOR TEMPERATURE $\cong$ 130° C; N = 3 x $10^{13}/cm^3$

- Noise fluorescence visible
- Investigate scaling w/density, pump intensity

90-12553a

Figure 2. Actively pumped rubidium cell.

• Noise detected at filter output wavelengths

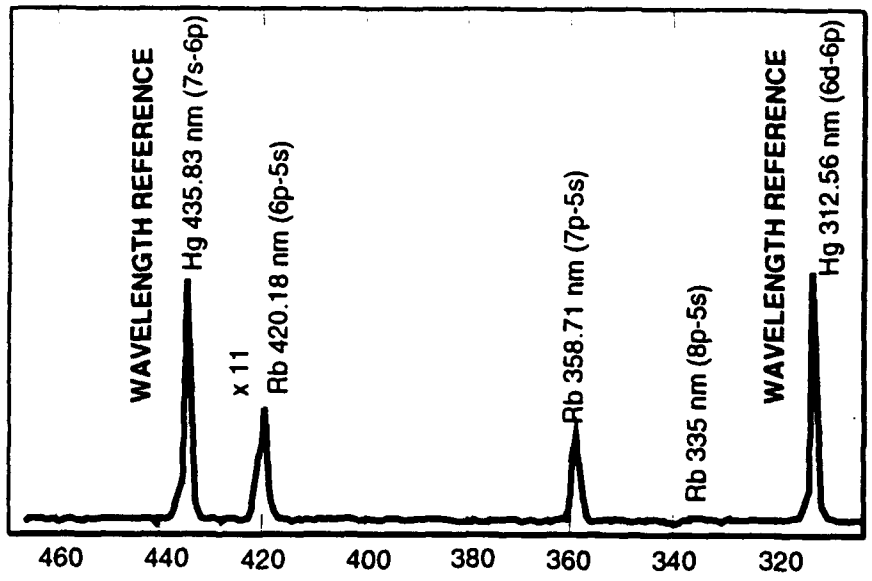

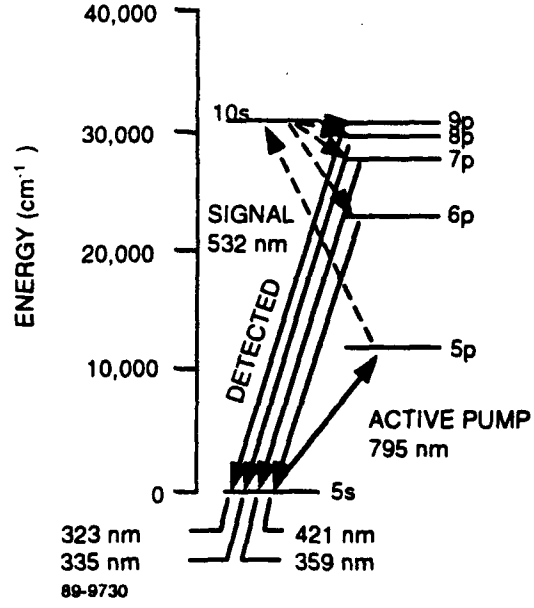

90-13056

Figure 3. Spectral profile of rubidium noise fluorescence.

- Intrinsic Noise Spectra
  Cesium Vapor
- Cell temperature: 126° C

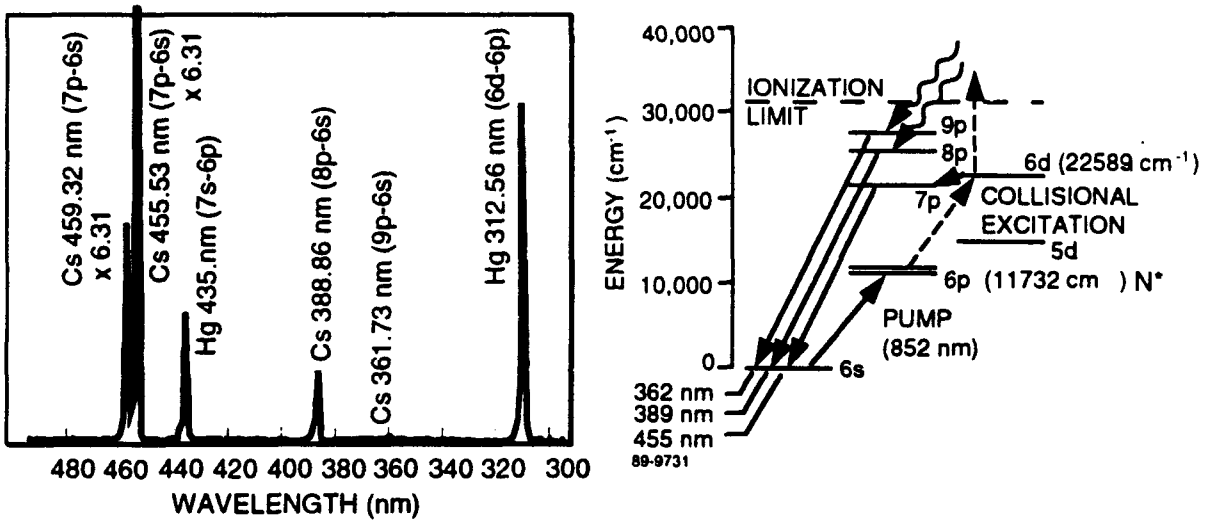

90-13057

Figure 4. Spectral profile of cesium noise fluorescence.

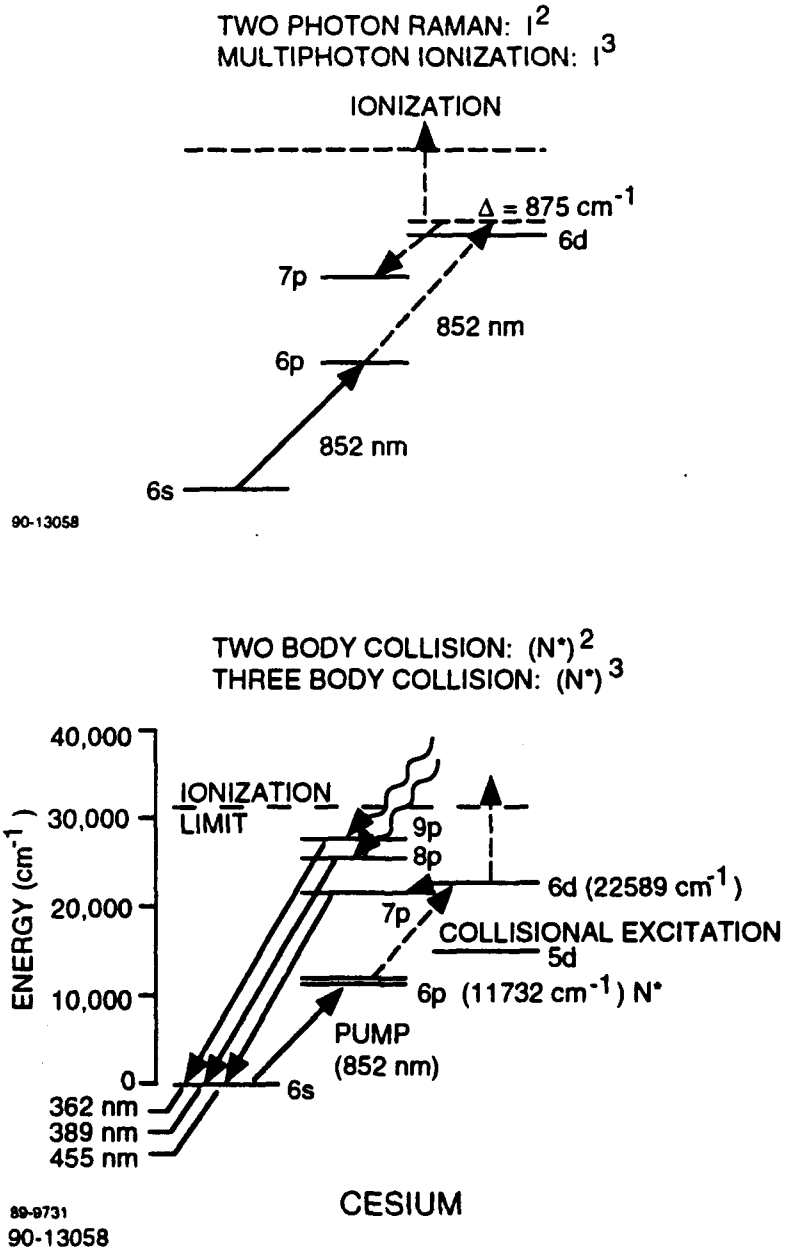

Figure 5. Possible mechanisms for noise generation in cesium.

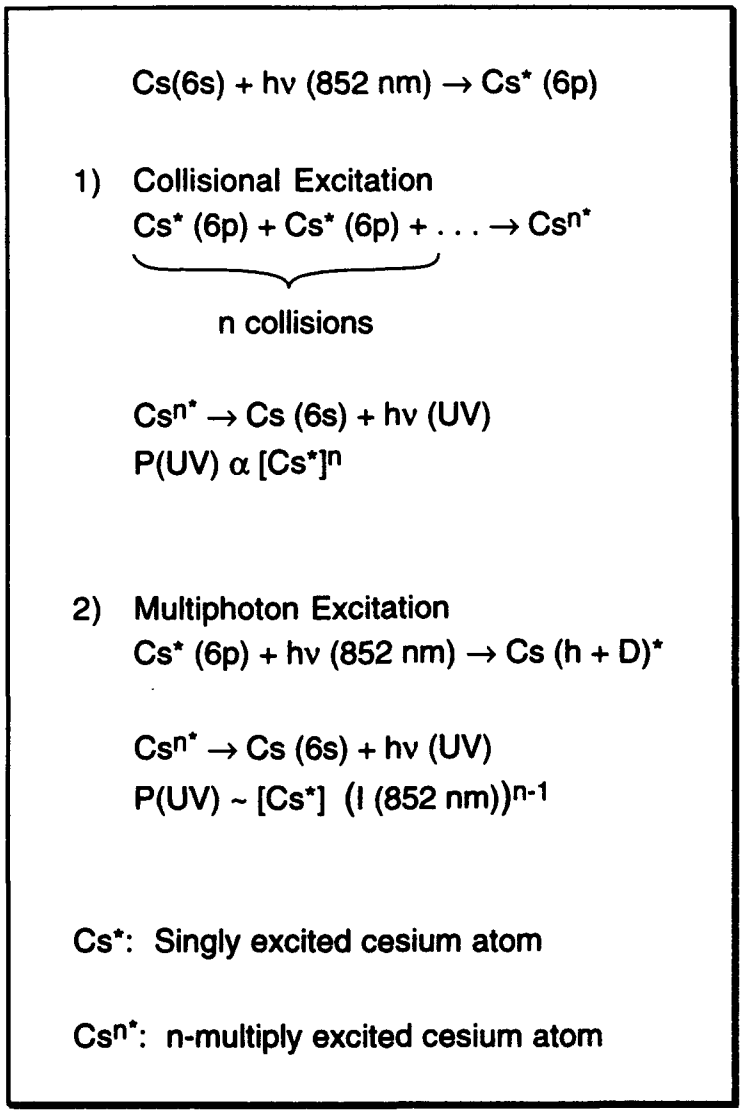

Figure 6. Excitation mechanisms.

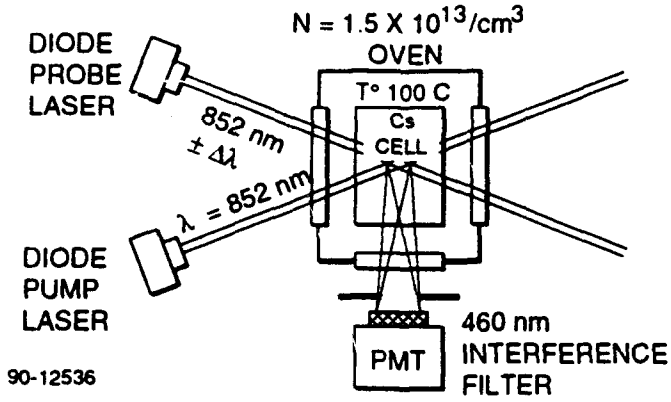

Pump laser: on resonance

P = 4.7 mW (in cell);
A = 2.5 x 10^{-3} cm^2
I = 1.9 W/cm^2

Probe laser: Scanning through resonance

P: 4 mW (in cell);
A = 2.5 x 10^{-3} cm^2
I = 1.6 W/cm^2

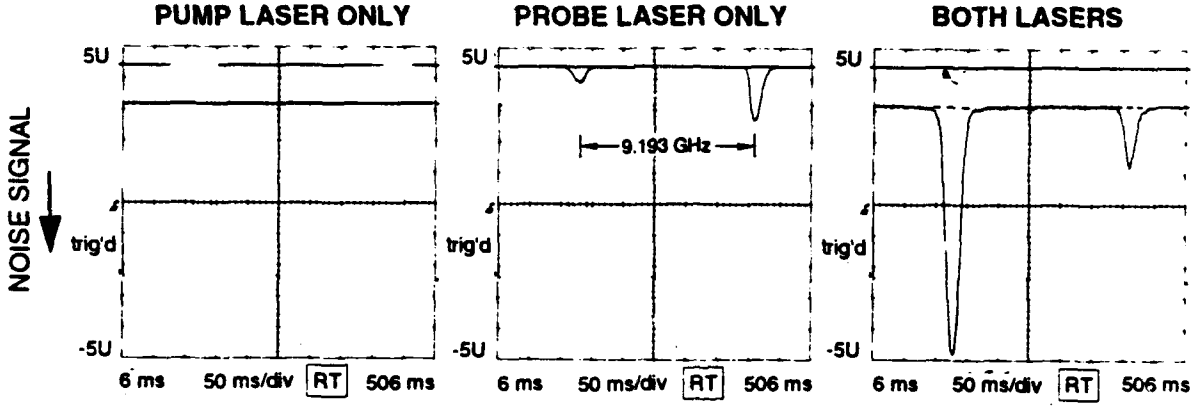

- Small detuning of probe laser from resonance should not eliminate multiphoton processes
- Noise is thus due to collisions

90-13059a

Figure 7. Intensity dependence experiment.

This page intentionally left blank.

3. Faraday Filter

Ultranarrow line filtering using a Cs Faraday filter at 852 nm

J. Menders, K. Benson, S. H. Bloom, C. S. Liu, and Eric Korevaar

Thermo Electron Technologies Corporation, 9550 Distribution Avenue, San Diego, California 92121-2305

Received January 28, 1991

To achieve quantum-noise-limited performance, background-limited laser receivers require narrow-band optical filters. We measured and modeled the ultranarrow-band transmission spectrum of a Cs Faraday filter at 852 nm. The transmission spectrum consisted of passbands on either side of the $6\,^2S_{1/2}$–$6\,^2P_{3/2}$ hyperfine doublet lines, making a total of four. The passbands may be simple peaks or highly modulated, depending on the operating parameters. We observed peaked passbands of near-unity transmission with a 0.6-GHz bandwidth and modulated bands with features as sharp as 100 MHz. Excellent agreement with our calculations at 852 nm allows us to predict confidently a 0.7-GHz transmission band for Cs at 455 nm.

To achieve quantum-noise-limited performance, background-limited laser receivers require narrow-band optical filters. Typically atomic line filters (ALF's) are used to obtain ultranarrow-band optical filtering,[1] achieving bandpasses of approximately 1 GHz. Another device, referred to as the Faraday filter,[2,3] the dispersive magneto-optic filter,[4] or the Faraday anomalous dispersion optical filter,[5] has been used to obtain bandpasses of approximately the same width. Faraday filters provide an optical passband at fixed wavelengths associated with strong atomic absorption lines as do ALF schemes. In addition, Faraday filters offer the advantages of near-unity peak transmission for linearly polarized light, image preservation,[6] and real-time operation (no excited-state decay delays). Although unpolarized light is limited to a peak transmission approaching one half, the combination of two filters in parallel can be used to provide near-unity transmission for each of the polarization components. Three early applications of Faraday filters were to high-speed optical modulation,[7] dye-laser frequency locking,[2,3] and the observation of solar sodium *D* lines.[8]

The filters can provide passbands either at or in the wings of the resonance for high (1 kG) or low (100 G) magnetic fields, respectively. In this Letter we present what are to our knowledge the most detailed transmission measurements and calculations for a Faraday filter operated in the wings of a resonance. For an optimally chosen field and temperature, the spectrum of a Cs Faraday filter exhibited two narrow strongly peaked 0.6-GHz passbands on either side of the atomic resonance at 852 nm. At higher temperatures and fields, rapid modulations appeared in the spectra. Like some previous analyses (Ref. 4, for example), ours began with a calculation of the atomic Zeeman spectrum. We refined the previous treatments by including the hyperfine interaction, obtaining excellent agreement with our measurements. Using the same modeling approach, we predict a 0.7-GHz passband for the optimal Cs filter spectrum at the 455-nm transition.

The construction of a Faraday filter is shown as a part of the experimental setup in Fig. 1. The filter consists of an alkali metal vapor in a magnetic field between crossed polarizers. As described below, the magnetic-field Zeeman splits the energy levels, resulting in separate absorption lines for left and right circularly polarized light. We can consider the filter transmission in terms of circularly polarized light outside, between, and at the absorption lines. Outside these lines, the filter can be regarded as a Faraday rotator that uses an alkali metal vapor as the magneto-optic material inserted between crossed polarizers. The metal vapor exhibits rotary power only in the immediate vicinity of an absorption line, providing the 90° turn needed to pass the second polarizer. A simple peaked transmission spectrum is obtained when the filter parameters are adjusted to provide a maximum rotation of 90°; at higher vapor densities and/or fields, multiple rotations lead to rapid modulations in the transmission spectrum. Away from the absorption line, the filter provides an out-of-band rejection determined by the extinction ratio of the crossed polarizers (typically $>10^5$). Under our operating conditions, both circular polarization components of light between the left and right circular lines are absorbed by the line wings. Light at either of the lines experiences preferential absorption of one circular polarization, producing circularly polarized light that is halved by the output polarizer.

Faraday filter transmission spectra were measured

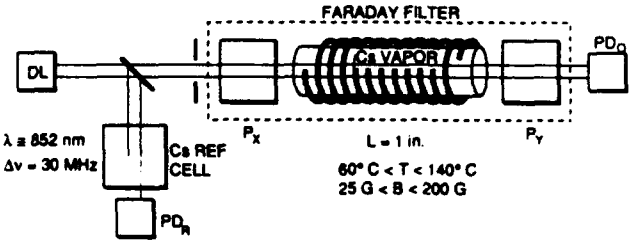

Fig. 1. Setup for high-resolution Faraday filter transmission spectrum measurement. The Faraday filter consists of the components enclosed by the dashed box. DL, diode laser; PD_R and PD_O, reference and output photodiodes, respectively; P_x and P_y, polarizers.

0146-9592/91/110846-03$5.00/0

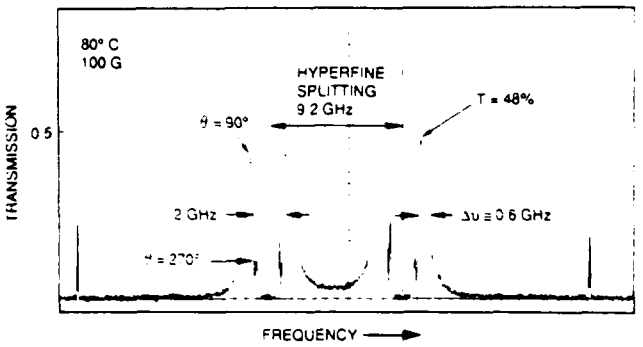

Fig. 2. Cs 852-nm Faraday filter transmission spectrum optimized for a laser receiver application. The magnetic field and the vapor temperature were chosen to produce a narrow bandpass with high transmission. Fresnel losses, which can be greatly reduced, accounted for 90% of the transmission losses.

for a range of fields and vapor densities using the setup shown in Fig. 1. A frequency-ramped, narrow-band beam provided by a current-modulated diode laser (Mitsubishi ML 2701) was split between the filter and a reference absorption cell. The filter[9] consisted of a 2.5-cm-long cell containing Cs vapor in a magnetic field provided by a coaxial solenoid sandwiched between two Glan–Thompson polarizers. The vapor density was determined by the regulated (±0.1°C) temperature of a cold finger in the cell, which ranged between 60 and 140°C, giving densities between 9.1×10^{11} and 1.3×10^{15} atoms/cm^3. The field was determined from a measure of the solenoid current using a factory-supplied calibration factor. We varied the current between 2 and 18 A to obtain fields of as much as 200 G. The filter and reference cell throughputs were monitored by silicon photodiodes, whose outputs were simultaneously displayed on an oscilloscope and dumped to a plotter.

An example of a useful transmission spectrum for laser receiver applications is represented by the data presented in Fig. 2. The narrow peak on the blue side of the spectrum has a bandwidth of 0.6 GHz and a peak transmission of approximately 48% compared with that of a cold filter (i.e., no vapor or field, with one uncoated polarizer removed) of approximately 54%. Thus, at this operating point, all the filter losses can be attributed to Fresnel losses, which can be reduced to a few percent by using antireflection coatings. The four passbands correspond to two pairs of passbands, one pair for each of the lines in the hyperfine doublet. This 9-GHz doublet appears in all passive Cs-based filters. The 2-GHz stop band between a pair of passbands is formed by the combination of absorption by the Doppler-broadened (0.4-GHz) left and right circular lines and a transmission null caused by a 180° rotation. As shown in Fig. 2, the transmission peaks occur for a 90° rotation, with an attenuated secondary peak for a rotation of 270°.

Additional measurements of transmission spectral variation with temperature and field showed the adjustability of filter bandwidth and position. A few examples from a series of measurements are presented in Fig. 3. The spectrum discussed above is the 100-G, 80°C case. As the 200-G column illustrates, the position of the primary passband is shifted away from line center as the vapor density is increased with temperature. The property could be useful for tracking Doppler-shifted signals from satellites. Note the development of a nearly square passband in the 200-G, 100°C case. This feature occurs because the nearly linearly decreasing circular birefringence from the two lines sum to a constant between the lines. The transmission is easily modulated by a 20-G change in the field, which offers the potential for use as a rapid beam modulator.

A convincing demonstration of the accuracy of our model can be made by using the complicated spectrum taken at 200 G and 120°C. A comparison between the measurement and our calculations is shown in Fig. 4. The coincidence of the modulation peaks and the shape of the primary passbands indicates that our model accurately predicts the rotation spectrum of the Faraday cell. The Faraday filter was analyzed in terms of a circularly birefringent, dichroic medium between crossed polarizers. The medium was characterized by the circular refractive indices n_σ and absorption coefficients α_σ, where $\sigma = +, -$ for left and

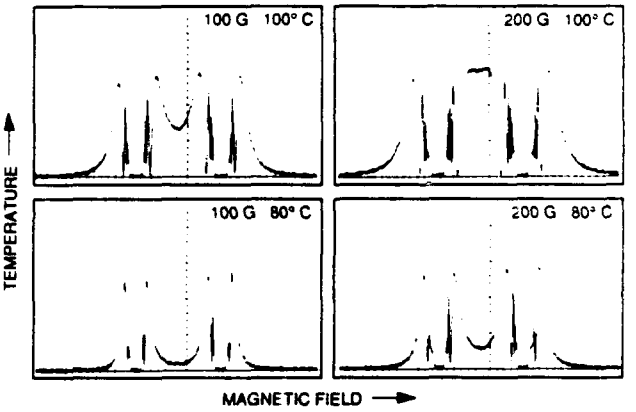

Fig. 3. Transmission spectrum variation for varying temperature and field strength. The passband position can be shifted by adjusting the temperature of the field. A square passband can be produced between the hyperfine splitting.

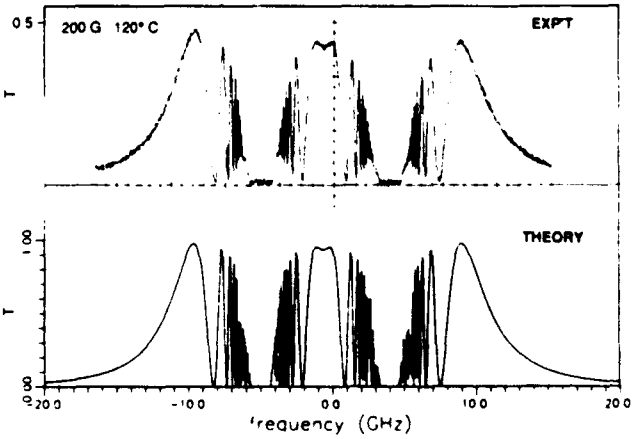

Fig. 4. Transmission spectrum in excellent agreement with the calculation. The coincidence of the transmission peaks shows the correspondence between the measured and calculated polarization rotation.

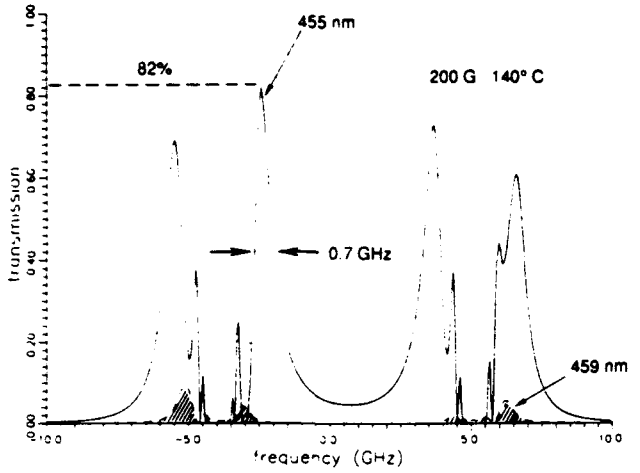

Fig. 5. Expected transmission spectrum at 455 nm. The operating parameters were chosen to give high transmission and narrow bandwidth at 455 nm while blocking transmission at the nearby 459-nm transition.

right circularly polarized light, respectively. The filter transmission is given by

$$T(\nu) = [\tfrac{1}{2}\exp(-\alpha_+ z) + \tfrac{1}{2}\exp(-\alpha_- z)]\sin^2\delta, \quad (1)$$

where

$$\delta(\nu) = \frac{\pi\nu z}{c}[n_-(\nu) - n_+(\nu)], \quad (2)$$

z is the Faraday cell length, and ν is the optical frequency. The $\alpha_\sigma(\nu)$ and $n_\sigma(\nu)$ are the sum of contributions from σ transitions in the vapor. The transition spectra and probabilities were determined by perturbing the fine structure states with the Zeeman and hyperfine interactions. The absorption coefficient due to a single transition from $|i\rangle$ to $|k\rangle$ for stationary atoms is

$$\alpha(\nu) = \frac{N\lambda_0^2}{8\pi}\frac{g_i}{g_k}A_{ik}\frac{\frac{\Gamma}{2\pi}}{(\Delta\nu)^2 + \left(\frac{\Gamma}{2}\right)^2}, \quad (3)$$

which gives, using the Kramers–Kronig relations,

$$n(\nu) - 1 = -\frac{N\lambda_0^3}{32\pi^3}\frac{g_i}{g_k}A_{ik}\frac{\Delta\nu}{(\Delta\nu)^2 + \left(\frac{\Gamma}{2}\right)^2}, \quad (4)$$

where N is the atomic density, ν_0 and λ_0 refer to the atomic transition frequency, g_i is the $2j + 1$ level degeneracy of state i, A_{ki} is the Einstein A coefficient, Γ is the natural linewidth, and $\Delta\nu = \nu - \nu_0$. These expressions were integrated over the Doppler distribution, and, finally, the total $\alpha_\sigma(\nu)$ and $n_\sigma(\nu)$ are found by summing the contributions from each of the σ transitions.

Using the same modeling approach, we produced the transmission spectra for the Cs 455- and 459-nm transitions shown in Fig. 5. The filter operating parameters were chosen such that the peak 455-nm transmission was maximized, while the area under the 459-nm spectrum was minimized to provide background rejection there. (Passive Cs ALF's for 455 nm also suffer from a similar background leak.) The result is a 455-nm filter with a peak transmission of 82% and a passband width of 0.7 GHz that substantially rejects background owing to the transition at 459 nm. Ultranarrow-band filters at this wavelength are useful for submarine laser communications.

In conclusion, the Cs Faraday filter has a 0.6-GHz passband near 852 nm. With the use of standard coating designs, the peak transmission (for polarized input light) should exceed 90%. The filter bandwidth and position were observed to be tunable over a range of approximately 5 GHz for possible applications to Doppler-shift compensation. Excellent agreement between our model and our measurements allowed us to predict confidently a 0.7-GHz transmission band for Cs at 455 nm.

The research presented here was partially supported by Office of Naval Research contract N00014-89-C-0068. We thank M. White of the Office of Naval Research, G. Beaghler of the Naval Ocean Systems Center, and G. Ferguson of the Naval Air Development Center for their encouragement and support.

References

1. J. A. Gelbwachs, IEEE J. Quantum Electron. **24**, 1266 (1988).
2. P. P. Sorokin, J. R. Lankard, V. L. Moruzzi, and A. Lurio, Appl. Phys. Lett. **15**, 179 (1969).
3. T. Endo, T. Yabuzoki, M. Kitano, T. Sato, and T. Ogawa, IEEE J. Quantum Electron. **QE-13**, 866 (1977).
4. P. Yeh, Appl. Opt. **21**, 2069 (1982).
5. T. Shay, in *Proceedings of the International Conference on Lasers '90*, D. G. Harris and J. Herbelin, eds. (STS, McLean, Va., to be published).
6. An image-preserving ALF was developed by E. Korevaar, M. Rivers, K. Choi, S. Bloom, K. Slatnick, and C. S. Liu, in *Proceedings of the International Conference on Lasers '89*, D. G. Harris and T. M. Shay, eds. (STS, McLean, Va., 1990), pp. 933–939.
7. B. M. Schmidt, J. M. Williams, and D. Williams, J. Opt. Soc. Am. **54**, 454 (1964).
8. G. Agnelli, A. Cacciani, and M. Fofi, Solar Phys. **44**, 509 (1975).
9. The Faraday filter was purchased from Shay-Blythe International, Las Cruces, N.M.

Blue cesium Faraday and Voigt magneto-optic atomic line filters

J. Menders, P. Searcy, K. Roff, and Eric Korevaar

Thermo Electron Technologies Corporation, 9550 Distribution Avenue, San Diego, California 92121-2305

Received June 11, 1992

We measured cesium magneto-optic line filter spectra at 455 nm for several field orientations. When optimized to achieve the narrowest passbands and the highest transmission, the Faraday filter (**B** along **k**) exhibited near-unity transmission peaks of 0.7-GHz bandwidth with an integrated transmission of ~3 GHz. A transmission calculation that includes the field angle was confirmed experimentally and used to show that the Faraday filter field of view is >60°. We devised a new type of magneto-optic atomic line filter that uses a transverse magnetic field, which we call the Voigt filter.

To achieve quantum-noise-limited performance, background-limited laser receivers require narrow-band optical filters. Laser communications and remote sensing have provided a strong impetus for the development of a variety of narrow-band filters, including those that operate in the blue-green for undersea applications. Magneto-optic atomic line filters known as Faraday filters have been shown to offer near-unity peak transmission and narrow passbands at discrete wavelengths associated with atomic transitions, especially those of the alkali metals.[1-3] For the blue-green region of the spectrum, a Ca filter was recently reported,[4] and a filter utilizing the blue Cs $6\,^2s_{1/2}$–$7\,^2p_{3/2}$ transition at 455 nm has been proposed and analyzed[1,5,6] but not demonstrated until now.[7]

In this Letter we report what are to our knowledge the first transmission spectrum measurements of a Cs Faraday filter operated in the wings of the resonance near 455 nm. We measured spectra under varying conditions designed to demonstrate optimal filter characteristics, check high-temperature operation, and anchor field-of-view calculations. We also describe what is to our knowledge the first transverse field magneto-optic filter, which we call the Voigt filter, after the Voigt effect.[8] A nonoptimal Voigt filter spectrum is presented, along with a calculation of an optimized Voigt filter. The Voigt filter provides a simple geometry when permanent magnets are used.

Both the Faraday and Voigt filters are based on the resonant birefringence induced in some atomic vapors by a magnetic field. The filters are constructed by sandwiching the birefringent vapor between crossed polarizers, so that only light experiencing a net polarization rotation of 90° is passed by the output polarizer. The required birefringence occurs close to the atomic absorption line, so that a passband is bounded by the absorption line on one side and the decay of the birefringence on the other. In the case of the Faraday filter, a magnetic field oriented along the axis of the filter gives rise to circular birefringence, which results in a gradual polarization rotation of a beam propagating through the vapor. On the other hand, a Voigt filter uses a transverse magnetic field, which gives rise to a linear birefringence. Voigt filter passbands are obtained by forming a resonant half-wave plate out of the vapor, oriented at 45° with respect to the input polarizer.

The left and right circular refractive indices, $n_{\sigma+}$ and $n_{\sigma-}$, are needed to analyze the Faraday filter. Calculations of these indices from atomic parameters can be found in the literature.[5,6] With an additional calculation of the n_π index, the dielectric tensor can be evaluated, and the polarization change for propagation through a vapor at an arbitrary angle to the magnetic field can be analyzed. In our approach, we began by assuming a form for the dielectric tensor that incorporates a gyration tensor in the Fresnel equation,[9] solved for the eigenindices in terms of the tensor elements, and evaluated the tensor elements using special cases. Here we use θ to denote the angle between the magnetic field and the wave vector and ϕ to denote the angle between the input polarization and the plane containing the field and the wave vector. Thus, for the Faraday filter, $\theta = 0$, and for the Voigt filter, $\theta = 90°$ and $\phi = 45°$. For the Voigt filter, we obtained the simple result that the eigenpolarizations are linear along and perpendicular to the magnetic field, with eigenindices n_π and $1/2(n_{\sigma+} + n_{\sigma-})$, respectively.

We measured blue Cs magneto-optic transmission spectra using the setup shown in Fig. 1. A 1-in. (2.5-cm) Cs vapor cell [0.8-in. (2-cm) vapor thickness], immersed in a uniform magnetic field provided by a Helmholtz coil, was sandwiched between crossed Glan–Thompson polarizers. The vapor density was determined by the temperature-regulated coldfinger in the cell. Measurements at various field angles were obtained by rotating the magnetic field (θ) and rolling the polarizers (ϕ) with the vapor cell held stationary. This approach was advantageous over rotating the cell and magnet as an assembly, in that it precluded Fresnel reflections by beams of uncertain polarization. A narrow-band

0146-9592/92/191388-03$5.00/0

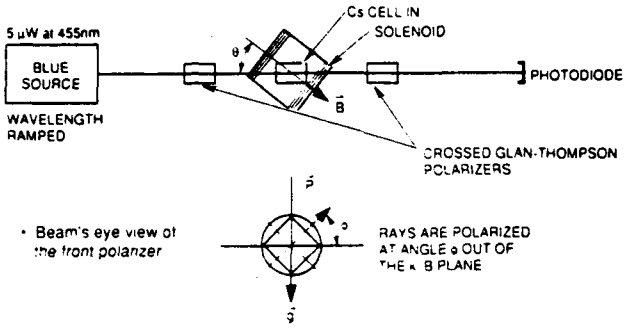

Fig. 1. Setup for measuring magneto-optic atomic line filter spectra.

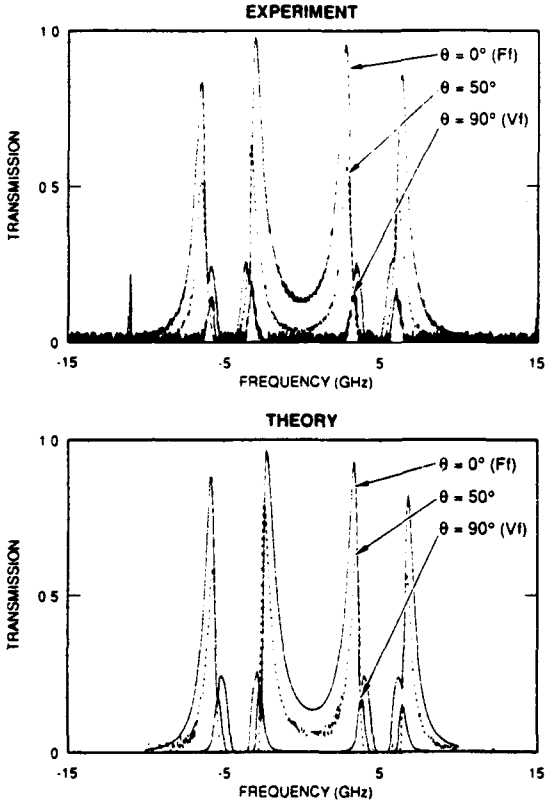

Fig. 2. Measured and calculated filter spectra for $\phi = 0°$ and $\theta = 0°$, 50°, and 90°. $\theta = 0°$ and 90° correspond to Faraday (labeled Ff) and Voigt (labeled Vf) filters, respectively. The 1-in. (2.5-cm) vapor cell [0.8-in. (2-cm) vapor thickness] was operated at 140°C and 200 G.

probe beam was obtained by doubling a diode laser operating near 911 nm. A current-modulated diode laser (Spectra Diode Laboratories device type S9130) emitted a frequency-ramped, narrow-band beam of ~50-mW power. The laser was isolated and focused into a 7-mm-long $KNbO_3$ doubling crystal mounted in an oven, which produced ~5 μW of blue light power. The beam was directed through the filter components and detected by a photodiode. To obtain properly normalized transmission spectra, we recorded throughput with the polarizers crossed and, subsequently, parallel. The transmission spectra presented below were calculated by normalizing the crossed data by the parallel data records.

We measured a near-optimum blue Cs Faraday filter transmission spectrum (labeled Ff in Fig. 2) with a peak transmission of ~97% (for input polarized light) and a low integrated transmission of ~3 GHz. The bandwidth of the tallest peak, ~0.7 GHz, is wide enough to transmit a matched single-mode laser beam. This spectrum was obtained with a magnetic field of ~200 G and a coldfinger temperature of 140°C, which gave a density of approximately 1.3×10^{14} atoms/cm^3. The four passbands consist of two pairs of passbands, each pair straddling a line of the Cs ground-state hyperfine doublet. The shape of the transmission spectrum is seen to match closely the theoretical spectrum exhibited in the plot below it. The differences in peak heights can be attributed to small amounts of birefringence in the cell windows.

At higher vapor temperatures, a broadening in the absorption lines appears to reduce the peak transmission. Consider the experimental and calculated spectra for filter operation at 200 G and 200°C shown in Fig. 3. The two spectra labeled by their linewidths Γ were calculated for Lorentzian broadenings of 1 (dotted curve) and 20 (solid curve) times the natural linewidth Γ_N (1.1 MHz) of the transition. A comparison between the two plots shows that the increased Lorentzian broadening led to a reduction in the height of the secondary peaks, which matched those of the data. We believe that the additional Lorentzian broadening is due to self-collisional broadening. Then the broadening at other temperatures can be found by scaling from the broadening at 200°C by using $\Gamma_{coll} \propto nT^{1.2}$, where n is the vapor density and T is the temperature.

The dependence of the filter transmission spectrum on field direction is shown in Fig. 3 for $\phi = 45°$. The three spectra were taken with the field along the filter axis (i.e., a Faraday filter), at 50° to the axis, and perpendicular to the axis (i.e., a Voigt filter). With the success of our off-axis filter calcu-

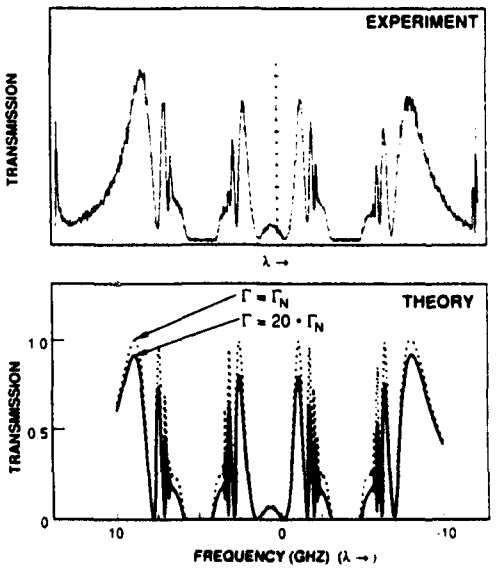

Fig. 3. Faraday filter spectra at 200°C and 200 G. The reduced transmission of the secondary peaks indicates the onset of additional Lorentzian broadening.

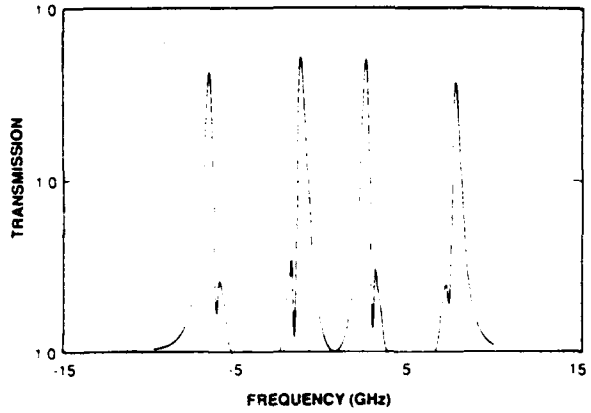

Fig. 4. Predicted optimal Voigt filter spectrum for a 1-in. (2.5-cm) cell at 180°C and 400 G.

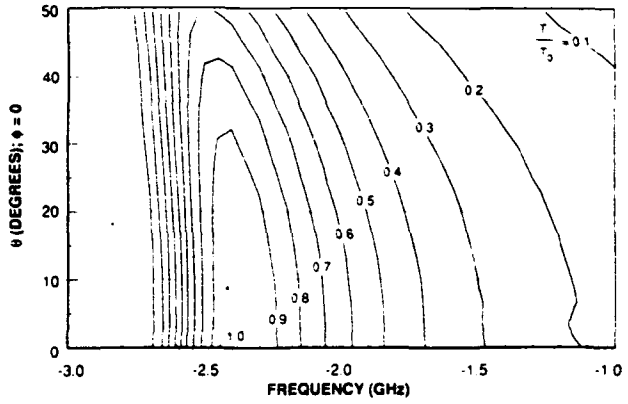

Fig. 5. Isotransmission contours showing filter passband spectrum variation with angle of incidence θ for $\phi = 0°$. The peak transmission is reduced by only 10% at a 30° angle of incidence.

lation confirmed by the close correspondence between the data and the calculated spectra (lower plots, Fig. 2), we continued our investigation of the Voigt filter and the Faraday filter field-of-view computationally. An optimal Voigt filter transmission spectrum, shown in Fig. 4, was achieved at a filter operating point of 400 G and 180°C with collisional broadening taken into account. Thus the Voigt filter can also provide near-unity peak transmission with a low integrated transmission, albeit at a significantly higher field and temperature than the comparable Faraday filter.

Off-axis Faraday filter spectrum calculations showed that the bandpass peak transmission, width, and position were largely insensitive to the field angle up to angles of >30° for the optimal filter. To analyze the filter field of view, the transmission spectra for a fan of rays with $\phi = 0°$ were calculated. The spectra in the vicinity of the maximum peak of a filter operated at 100 G and 160°C were combined to produce the isotransmission contour plot presented in Fig. 5. The contours show that a narrowband beam tuned to the on-axis transmission peak experiences only a 10% reduction in transmission for angles of incidence out to ~30° off axis. In addition, neither the filter bandwidth nor the position is significantly altered. Finally, the passband spectrum at $\theta = 30°$ was found to be independent of ϕ to within a few percent, which established a 60° field of view.

In summary, we have shown that near-unity peak transmission, low integrated transmission, and 1-GHz bandwidths can be provided by the ultranarrow-band blue Cs Faraday and Voigt filters at 455 nm. In addition, we found a wide Faraday filter field of view of 60°.

The research presented here was partially supported by U.S. Office of Naval Research contract N00014-89-C-0068 and Naval Air Warfare Center (NAWC) contract N62269-90-C-0516. We thank G. Beaghler and G. Adams of the Naval Ocean Systems Center and M. Conterino and W. Scharpf of NAWC for their encouragement and support.

References

1. J. Menders, K. Benson, S. H. Bloom, C. S. Liu, and E. Korevaar, Opt. Lett. **16,** 846 (1991).
2. D. J. Dick and T. M. Shay, Opt. Lett. **16,** 867 (1991).
3. T. Endo, T. Yabuzoki, M. Kitano, T. Sato, and T. Ogawa, IEEE J. Quantum Electron. **QE-13,** 866 (1977).
4. J. A. Gelbwachs and Y. C. Chan, in *Conference on Lasers and Electro-Optics,* Vol. 12 of 1992 OSA Technical Digest Series (Optical Society of America, Washington, D.C., 1992), p. 538.
5. P. Yeh, Appl. Opt. **21,** 2069 (1982).
6. B. Yin and T. M. Shay, IEEE Photon. Technol. Lett. **4,** 488 (1992). We caution that our model does not reproduce the spectra predicted by this reference.
7. J. Menders, P. Searcy, K. Roff, S. H. Bloom, and E. Korevaar, in *Conference on Lasers and Electro-Optics,* Vol. 12 of 1992 OSA Technical Digest Series (Optical Society of America, Washington, D.C., 1992), paper CPD3.
8. F. A. Jenkins and H. E. White, *Fundamentals of Optics* (McGraw-Hill, New York, 1957), pp. 599–601.
9. A. Yariv and P. Yeh, *Optical Waves in Crystals* (Wiley, New York, 1984), p. 97.

Sodium-vapor dispersive Faraday filter

H. Chen and C. Y. She

Department of Physics, Colorado State University, Fort Collins, Colorado 80523

Paul Searcy and Eric Korevaar

ThermoTrex Corporation, 9550 Distribution Avenue, San Diego, California 92121

Received December 3, 1992

Ultranarrow bandpass Na vapor dispersive Faraday filters at 589 nm are studied experimentally and theoretically. Their anticipated performance in the line-center operation is demonstrated experimentally with a thin Na cell in an axial magnetic field of 1750 G. A peak vapor transmission of 85%, a FWHM linewidth of 0.002 nm (or 1.9 GHz), and a background transmission of 2×10^{-5} have been achieved.

Narrow-band filters are necessary in free-space optical communication to extract narrow-band signal in the presence of a broadband optical background. Conventional interference filters cannot provide extremely narrow bandwidths (0.001–0.1 nm) with a highly stable transmission peak and a reasonably large field of view. Various schemes, including atomic resonance filters,[1] have been proposed and demonstrated.[2] The idea of using a circularly birefringent, dichroic medium between crossed polarizers as such a filter, first introduced and demonstrated by Ohman,[3] has recently been revived[4] and actively pursued[5–7] for laser-based applications. In addition to the atomic resonance filter properties of wide field of view, high background rejection ratio, and stable transmission characteristics, a Faraday filter based on anomalous dispersion has a fast time response and near-unity peak transmission.[4]

Dick and Shay[4] were the first to revisit the vapor Faraday filter for modern applications by investigating the filter transmission of the Rb $5s-5p$ hyperfine doublet transition near 780 nm. Menders *et al.*[5] immediately investigated the hyperfine doublet of the Cs $6s-6p$ transition at 852 nm by performing both theoretical and experimental studies with axial magnetic fields of 100 and 200 G. Their experimental result agrees in great detail with the theory that takes the quantum-mechanical aspects fully into account. The theory was independently published by Yin and Shay[7] and by Peng *et al.*[8] Chan and Gelbwachs demonstrated filter operation at a Fraunhofer wavelength[6] by exploiting the Ca $4s-4p$ transition near 422.7 nm. These experimental studies were carried out under relatively weak magnetic fields, and thus only the operation in the wings has been investigated. In these cases, two sets of transmission peaks well separated by the hyperfine splitting of the transition were observed. In this Letter we present a study of Na Faraday filters under a strong axial magnetic field of 1750 G, which thereby achieves line-center operation. A peak vapor transmission (apart from the losses arising from the optical components) of 85% at the line center of the Na D_2 transition ($\lambda = 589.0$ nm), a FWHM linewidth of 0.002 nm (or 1.9 GHz), and a background transmission of 2×10^{-5} have been achieved. Simulations with the inclusion of hyperfine interaction and a magnetic field between 1500 and 2000 G with the use of a strong-field approximation for the quartet Na excited state, $3^2P_{3/2}$, were compared with the measured transmission functions, quantitatively with high spectral resolution and precision.

In 1975, a Na Faraday filter in a magnetic field of 1500 G was in fact constructed by Agnelli *et al.* for the observation of solar sodium D lines.[9] They performed theoretical calculations that included hyperfine splitting, but their theory can be compared with their observations only qualitatively, owing to the lack of experimental resolution. Their filter gave a total full width of 0.016 nm and a maximum transmission of 25%. The predicted narrower width and near-unity vapor transmission were not realized. The Na Faraday filter described here has a much narrower full width of 0.002 nm, which is suitable for the daytime operation of a Na temperature lidar,[10] a topic of current interest.

The experimental scheme is shown in Fig. 1. A dye laser is used as the light source, and a Fabry–Perot interferometer is used as the frequency marker. The absolute frequency of the Na D_1 and D_2 transitions is determined by the Doppler-free fluorescence spectra[11] from a simple Na cell (not shown) taken simultaneously. Two detectors (Det. 1 and Det. 2) monitor, respectively, the laser intensity and the signal transmitted through the filter. The filter consists of two crossed polarizers, P1 and P2, and a Na cell (0.76 cm long and 2 cm in diameter) in an axial magnetic field of 1750 G produced by four rare-earth magnets (5 cm × 5 cm × 1.2 cm each) arranged to create a magnetic field parallel to the optical axis at the cell location. Heated by an aluminum ring, the sodium cell is held in a Teflon oven.

The filter transmissions near the D_1 and D_2 line centers as a function of frequency were measured for three different cell temperatures, 181, 185 and 189 °C, with the 189 °C case shown in Fig. 2(a). The filter transmission is determined from the ratio of two measured intensity ratios (Det. 2 to Det. 1); the

0146-9592/93/121019-03$6.00/0

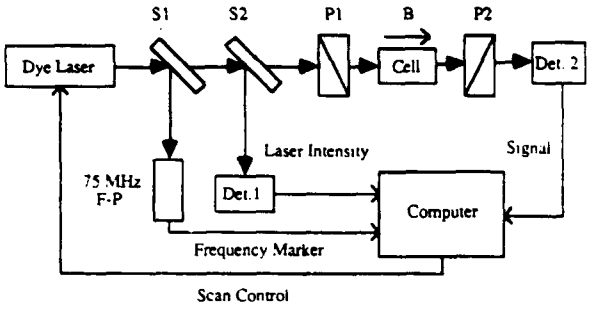

Fig. 1. Experimental setup for measuring the filter transmission. The Na vapor cell is held in a Teflon oven, where four rare-earth permanent magnets are arranged so that the magnetic field at the cell position is axial. F-P, Fabry–Perot interferometer; S1, S2, beam splitters; B, magnetic field.

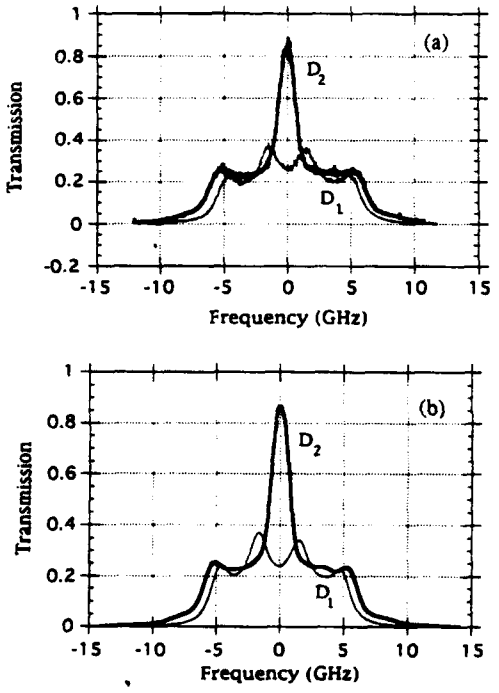

Fig. 2. (a) Experimental and (b) theoretical filter transmissions for D_1 and D_2 lines in an axial magnetic field of 1750 G with a cell, 0.76 cm long, at 189 °C.

numerator is the intensity ratio at the frequency of interest when the polarizers, P1 and P2, are set perpendicular to each other as required for the filter operation, and the denominator is the intensity ratio off resonance (by 0.3 nm, for example) when the polarizers, P1 and P2, are set parallel to each other. At the line center, the transmission function of the D_2 line has its peak value, whereas it shows a dip for the D_1 line. The peak transmission of the D_2 line is higher than that of the D_1 line by more than a factor of 2. As the cell temperature increases, the transmissions for both D_1 and D_2 lines increase and the linewidth of the D_2 line decreases. The measured peak transmission, the FWHM linewidth, and the equivalent noise bandwidth for all three temperatures are given in Table 1, along with the associated theoretical values. The effective optical depth of the filter, τ, is defined as $Ne^2|f|L/\sqrt{\pi}(dw_d)mc\epsilon_0$, where f, L, and (dw_d) are, respectively, the emission oscillator strength, the cell length, and $\sqrt{2}$ times the rms Doppler width of the transition. The calculated and measured values are in good agreement. In addition to the extinction of the crossed polarizers, the background transmission depends more critically on the temperature-dependent birefringence of the cell window. At the operation temperatures, we measured the background transmission to be 2×10^{-5}.

The theory of a vapor dispersive Faraday filter has been described previously[2,4,7–9] and is not repeated here. To obtain the numerical results for the D_1 and D_2 transitions, we solve the eigenvalue problem of a Na atom in an axial magnetic field including the hyperfine interaction for the $3^2S_{1/2}$, $3^2P_{1/2}$, and $3^2P_{3/2}$ manifolds separately; a rough estimate of the ratio of hyperfine to Zeeman energies, DH_{hfs}/DH_{Zeeman}, gives $320/B$, $100/B$, and $10/B$, respectively, where B is the axial magnetic field in Gauss. Because the field strength of interest is between 1500 and 2000 G, we solve the eigenvalue problem for $3^2S_{1/2}$ and $3^2P_{1/2}$ manifolds exactly and use the strong-field approximation for the $3^2P_{3/2}$ manifold. The calculated transmission function for the cell temperature of 189 °C and magnetic field of 1750 G is shown in Fig. 2(b), which is in good agreement with the measured results shown in Fig. 2(a). The agreement holds for cell temperatures of 181 and 185 °C as well. The filter parameters for all three cases are compared in Table 1. Using the existing code for the $I = 3/2$ case,[5] we have also calculated the transmission function for the case of 1750 G and 189 °C exactly and found it to be in complete agreement with result based on a strong-field approximation for the $3^2P_{3/2}$ manifold.

To understand the transmission functions of the line-center operation for D_1 and D_2 transitions in

Table 1. Experimental and Theoretical Na Faraday Filter Characteristics for the D_1 and D_2 lines in an Axial Magnetic Field of 1750 G

	Temperature	Effective Optical Depth τ	Peak Transmission (%)		FWHM (GHz)		Equivalent Noise Bandwidth (GHz)
			Experimental	Theoretical	Experimental	Theoretical	
D_1	181	2.56	19	21	10.2	10.2	8.2
	185	3.36	28	29	9.9	10.2	8.4
	189	4.21	37	37	10.5	10.4	8.3
D_2	181	2.56	58	58	3.4	3.4	5.2
	185	3.36	76	78	2.5	2.4	5.0
	189	4.21	85	85	1.9	1.8	5.1

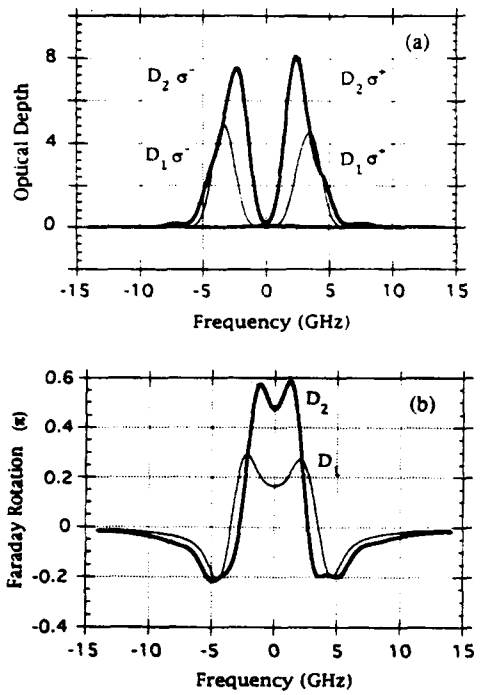

Fig. 3. Calculated (a) optical depth $\alpha_{\pm}L$ (not to be confused with τ) and (b) Faraday rotation (angle) for the σ^+ and σ^- transitions of the D_1 and D_2 lines of a Na cell, 0.76 cm long, in an axial magnetic field of 1750 G at 189 °C.

more detail, we plot the optical depth, $\alpha_{\pm}L$ (not to be confused with τ, with $\alpha_{\pm}$ being the absorption coefficient), and the angle of Faraday rotation for the σ^+ and σ^- transitions as shown in Figs. 3(a) and 3(b). As mentioned above, under a strong B field, σ^+ and σ^- absorption peaks are separated from each other, showing negligible circular dichroism at the line center. The transmission is determined mainly by the Faraday rotation, which shows a dip in the center owing to the fact that the Zeeman shift, ~3.3 GHz, is larger than the FWHM Doppler linewidth by more than a factor of 2. For the D_1 transition the absorption peaks occur farther away from the line center than do the peaks of the Faraday rotation, which leads to four resolvable peaks in the transmission function. There are four peaks in the profile of the D_2 absorption coefficient because the total electron angular momentum of the excited state is 3/2. The two peaks that have larger transition matrix elements are closer to the line center, ~2.4 GHz away. This combination gives a Faraday rotation for a strong peak in the line center plus two weak satellite peaks in the transmission.[2] Under a proper setting of cell temperature, the two satellite peaks may be suppressed as the strong dichroism overlaps the extrema in Faraday rotation. With large dichroism occurring near the strong D_2 absorption peaks, ±1.5 to ±3.5 GHz from the line center, one circularly polarized component is nearly completely absorbed, while the other component totally transmitted, giving a filter transmission of roughly 25%. Since the oscillator strength of the D_1 line is half as large as that of the D_2 line, the D_1 line has a smaller Faraday rotation, thus a lower peak transmission. As is shown in Fig. 3(b), if the Faraday rotation angle at the center of D_2 line is $\sim\pi/2$, the transmission of D_2 will decrease if we increase the vapor density. A higher magnetic field would be needed for the peak transmission to exceed 85%. However, if the rotation at the line center of the D_1 transition is only 0.16π, its peak transmission will continue to increase as the Na density increases. Since the hyperfine splitting of the Na ground state is only 1.7 GHz, comparable with its Doppler broadening, unlike for the case of Cs,[4,7] the behavior of the Na filter transmission function is qualitatively the same as the case without hyperfine splitting, which was considered by Yeh.[2]

In conclusion, we have demonstrated the expected line-center operation of an ultranarrow bandpass vapor dispersive Faraday filter. With a Na cell of 0.76 cm in length in an axial magnetic field of 1750 G, the peak transmission has reached 85% with a FWHM bandwidth of only 1.9 GHz. The background transmission off resonance has been blocked to a level of 2×10^{-5}. Theoretical and experimental results are in good agreement for both D_1 and D_2 transitions. Since the hyperfine energy is less than 0.7% of the Zeeman energy for the quartet Na excited state, $3^2P_{3/2}$, in a magnetic field greater than 1500 G, the strong-field approximation may be used in calculation for this manifold. In addition to free-space communication, a unique application for a narrow bandpass filter at Na resonance is to block effectively the broadband sunlit sky background to aid the observation of solar sodium D lines[9] and for the daytime operation of a Na temperature lidar.[10]

The research at Colorado State University was done with the experimental assistance of J. R. Yu and was partially supported by National Science Foundation grant ATM-91-01842. The research at ThermoTrex was conducted under Strategic Defense Initiative Organization/SSDC contract DASG60-89-C-0120 and U.S. Office of Naval Research contract N00014-89-C-0068 and with the support of Kepi Wu, John Johnson, and Guy Beaghler.

References

1. J. A. Gelbwachs, IEEE J. Quantum Electron. **24,** 1266 (1988).
2. P. Yeh, Appl. Opt. **21,** 2069 (1982).
3. Y. Ohman, Stockholm Obs. Ann. **19,** 3 (1956).
4. D. J. Dick and T. M. Shay, Opt. Lett. **16,** 867 (1991).
5. J. Menders, K. Benson, S. H. Bloom, C. S. Liu, and E. Korevaar, Opt. Lett. **16,** 846 (1991).
6. Y. C. Chan and J. A. Gelbwachs, IEEE J. Quantum Electron. (to be published).
7. B. Yin and T. M. Shay, Opt. Lett. **16,** 1617 (1991).
8. Y. F. Peng, J. X. Tang, and Q. J. Wang, Acta Phys. Sinica **2,** 39 (1992).
9. G. Agnelli, A. Cacciani, and M. Fofi, Solar Phys. **44,** 509 (1975).
10. C. Y. She, H. Latifi, J. R. Yu, R. J. Alvarez II, R. E. Bills, and C. S. Gardner, Geophys. Res. Lett. **17,** 929 (1990).
11. C. Y. She, J. R. Yu, H. Latifi, and R. E. Bills, Appl. Opt. **31,** 2095 (1992).

4. Locked Laser

Optics Communications 88 (1992) 385–390
North-Holland

OPTICS
COMMUNICATIONS

A Q-switched alexandrite laser injection seeded by a rubidium absorption frequency matched diode laser

K. Choi, S.H. Lin, Eric Korevaar and C.S. Liu
Thermo Electron Technologies, 9550 Distribution Avenue, San Diego, CA 92121, USA

Received 25 August 1991

We developed a narrowband Q-switched alexandrite laser injection seeded by a diode laser which was frequency stabilized to the 780 nm rubidium atomic absorption line. We were able to get injection seeded single-mode output pulses of ~ 10 mJ per pulse energy at 780 nm with ~ 200 ns fwhm pulse duration. By using a side injection scheme and an active cavity length control technique high efficiency injection locking was obtained with small injection power. This system was used as an illumination source for atomic line filters with excellent long term stability and day-to-day reliability.

1. Introduction

The alexandrite laser can be tuned to match the atomic absorption wavelengths in potassium and rubidium which are useful materials for atomic line filters [1]. Atomic line filters using potassium require signal photon wavelengths of 767 or 770 nm while a rubidium filter requires 780 nm signal photons. All these wavelengths are covered by an alexandrite laser's tuning range. For remote target detection in which a laser beam is scattered off of an object and the return signal is detected, the transmitted power requirement is generally high enough to require a pulsed laser. And, to be useful for the atomic line filter applications the signal laser bandwidth needs to be smaller than the Doppler width of the atomic transition so that most of the signal photons are absorbed in the atomic vapor cell. The power and bandwidth requirements for many applications can be met by using a Q-switched alexandrite laser injection seeded by a single mode cw diode laser locked to an atomic or molecular absorption feature at the wavelength of interest.

Injection seeding – which is the term used for pulsed lasers – and injection locking – the term used for cw lasers – is a technique by which a low-power laser with desirable frequency and spatial properties (the master) is used to impose its good characteristics onto a high power laser (the slave) whose spectral and spatial properties would otherwise not be so good [2]. By injecting the master laser output beam into the slave laser cavity the high power slave laser can have a single mode laser output without the use of etalons or other intra-cavity line selecting elements. Previous reports on injection seeding of an alexandrite laser used end injection schemes in which the diode laser beam was injected through the high reflecting end mirror [3] or the output coupler [4]. We report here the use of a side injection scheme in which the rubidium absorption frequency matched diode laser beam is injected into the resonance condition matched alexandrite oscillator from the side through a polarizing beam splitter to provide a large number of injecting photons during the early stages of the Q-switch pulse buildup.

2. Theory

The cavity field equation when the injection seeding beam is present [5] is

$$dE_\omega(t)/dt = m(t)\,E_\omega(t) + \{m(t)/\exp[2\tau\, m(t)-1]\}E_{i\omega}(t)\,. \quad (1)$$

In this equation $E_{i\omega}$ is the injected field with frequency ω, E_ω is the cavity field at the injected frequency ω, $m(t)$ is the time dependent gain term in

the laser cavity (per unit time), and 2τ is the cavity round trip time. During the initial buildup stage, when $m(t)$ is small, the field is driven mainly by the second term which is the Fabry–Pérot modulated injection field. When the gain is larger than the loss and m becomes large, the first term, which is the amplification term, soon dominates over the second term. Hence, the influence of the injected field on the cavity field is important only during the initial buildup time of the slave oscillator. Numerical studies [5] detailing eq. (1) show that when there is a frequency mismatch between the frequency of the injected field and the cavity resonance frequency, the injection field undergoes a rapid phase change which causes the field frequency to shift toward the nearest axial mode of the slave oscillator during the amplification process. In other words, the output frequency is determined by the slave oscillator, not by the master oscillator. The detuning range for single axial mode operation is defined as the frequency detuning range over which the output power ratio between the seeded axial mode and the non-seeded adjacent axial mode always exceeds an arbitrary set value.

3. Experimental detail

Fig. 1 shows a schematic of the experimental setup used in the injection seeding demonstration. The whole setup can be divided into the alexandrite laser, the injection seeder and the interfacing optics. The slave oscillator is a modified SEO (Schwartz Electro Optics) laser 1-2-3 alexandrite laser which is tunable from 720–790 nm. The laser rod size is 5 mm diameter × 75 mm length with 0.12% atomic weight Cr concentration. The charging unit supplies the charging current and voltage to a PFN with a 1000 J/s charging capacity. The PFN charging capacitance is 200 μF. Cooling is done by circulating deionized water with a Neslab circulator with 1 gpm flow rate at 60 psi pressure. The Q-switch is a KD*P crystal with 780 nm AR coated windows and a quarter-wave ($\lambda/4$) voltage of 2.4 kV. The total length of the cavity is 65 cm. The output coupler is a 80% reflective flat mirror and the rear mirror is a 98% reflective concave mirror with 5 meter radius of curvature. A three plate birefringent filter with a 1:2:10 thickness ratio (1 corresponds to a 0.5 mm thickness quartz plate) is used to tune the laser to 780 nm.

The alexandrite laser rod is a biaxial crystal with three crystallographic axes. The c-axis is parallel to the optic z-axis and the b-axis is set parallel to the laser beam polarization direction since the laser gain with b-axis parallel to the E-field ($b \| E$) is ten times higher than for $a \| E$. Perfect parallelism between b and E is very important since the residual birefringence due to a mismatch between E-field polarization direction and the b-axis prevents continuous tuning of the laser [6].

The injection seeding source is a gain guided diode laser (Mitsubishi ML 4102) emitting 3 mW output power at 780 nm with <30 MHz linewidth. The wavelength tunability of this diode laser is 0.016 nm/mA for bias current tuning and 0.22 nm/°C for temperature tuning. The output frequency of the diode laser is locked to an atomic rubidium absorption line by using a reference rubidium cell, a small wavelength modulation, and an electronic feedback circuit. In this experiment, we used the strongest absorption maximum of the rubidium $5s_{1/2} \rightarrow 6p_{3/2}$ hyperfine transitions at 780 nm. The linewidth of the laser was determined to be ~ 30 MHz (fwhm) from interferometric fringe visibility measurements. The diode laser is powered by a battery operated ultra low noise current source (ILX Lightwave LDX-3620) and its temperature is controlled by a thermoelectric temperature controller which has better than 0.01°C stability and ± 0.2°C accuracy. The diode laser is mounted in a temperature controlled laser diode mount which includes a thermoelectric cooler and a lens assembly for beam collimation. A Faraday isolator is used to block unwanted alexandrite laser light from reaching the diode laser.

The s-polarized diode laser beam is injected into the alexandrite cavity from the side. Before Q-switching, the s-polarized injection beam becomes p-polarized after passing the quarter wave plate twice and thus passes through the alexandrite rod. When, as a result of Q-switching, the quarter wave plate is nullified by the Q-switch, the s-polarized injection seeding beam will not reach the alexandrite rod. During the Q-switch build up period, the laser cavity losses decrease (allowing buildup of laser oscillation) at the same time that the injected power in the

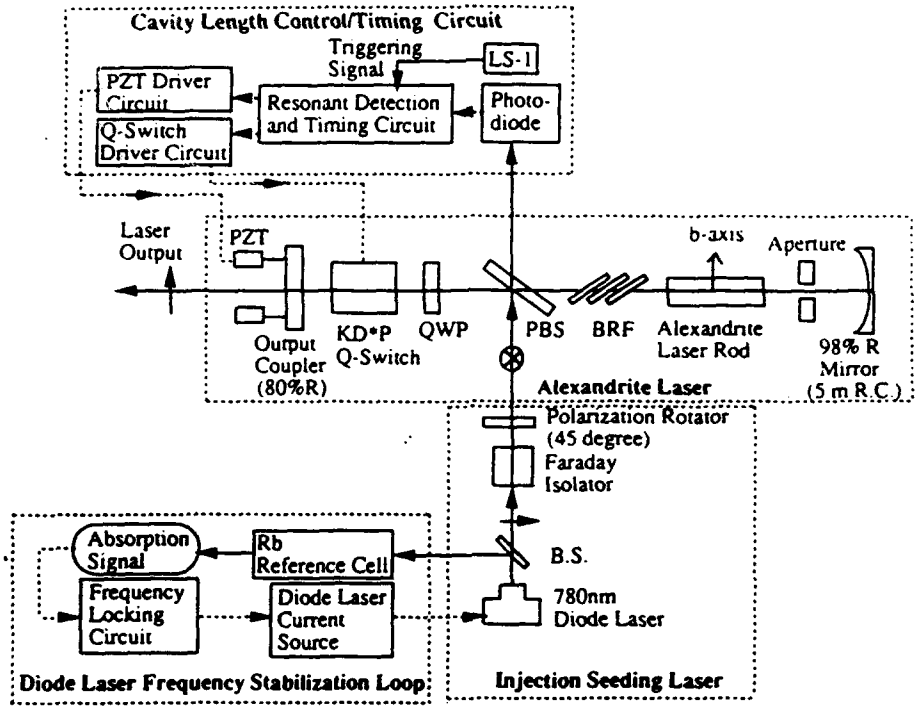

Fig. 1. The experimental setup used to demonstrate injection seeding.

rod decreases. However a good portion of the injection beam still reaches the laser rod during this time and hence provides the injection field which is effective during the early stages of the Q-switching build-up time and is very crucial for successful injection seeding. The side injection scheme provides a large amount of injection photons during the early stage of Q-switch pulse buildup and good isolation between the injection seeder and the alexandrite laser.

To satisfy the Fabry–Pérot boundary condition in the slave laser resonator the total length of the cavity should be an integer multiple of the wavelength of the injection seeding laser beam. The injection seeded laser frequency can jump from one cavity resonance frequency to another cavity resonance frequency without this cavity length control which is detri mental for atomic line filter applications. Locking the cavity length on a cw basis did not work because the length of the alexandrite rod changed up to 5λ during the flashlamp pumping pulse. Instead, to control the length of the laser cavity we used a pulsed scheme [7] in which a ramp signal moves a PZT mounted output coupler mirror for two free spectral ranges after a sufficient population inversion is built up in the laser rod. The Q-switch firing time is determined by monitoring the interference signal of the injection seeding laser beam which goes through the beamsplitter and that which makes a round trip in the cavity. When the cavity resonance frequency matches the diode laser frequency a maximum in the interference signal is obtained and the Q-switch is triggered. Since the Q-switch fires on a time scale much less than that of the moving mirror, the cavity length is optimum and basically constant during the laser pulse.

4. Verification of injection seeding

Injection seeding was verified by monitoring the alexandrite wavelength on a Candela LS-I spectrometer, and the bandwidth with a Fabry–Pérot interferometer. Single mode operation could be verified from the time response. Long term stability was

monitored while using the laser in an experiment requiring absorption in rubidium vapor. Candela LS-1 wavelength output of the unseeded and seeded alexandrite laser is shown in fig. 2. The unseeded beam shows a distribution of laser output energy over a 20 GHz range, while the seeded beam output is limited by the spectrometer resolution. For this experiment a seeding power of 10 μW was used. Narrowband lasing for injected power as low as 2 μW was observed. In fig. 3, the Fabry–Pérot interferograms of the injection seeded output spectra show single longitudinal mode oscillation while the unseeded spectra show multimode oscillation which washed out the interference rings. It is expected that the linewidth of the alexandrite a laser beam is equal to that of the diode laser beam since the transform limited linewidth of the alexandrite laser beam for a 200 ns fwhm pulse duration is ~1 MHz which is much smaller than the diode laser bandwidth of 30 MHz.

In fig. 4 output temporal waveforms of the *Q*-switched alexandrite laser are shown. Waveform (a) shows single mode oscillation with injection seeding while waveform (b) shows a pulse with mode beat-

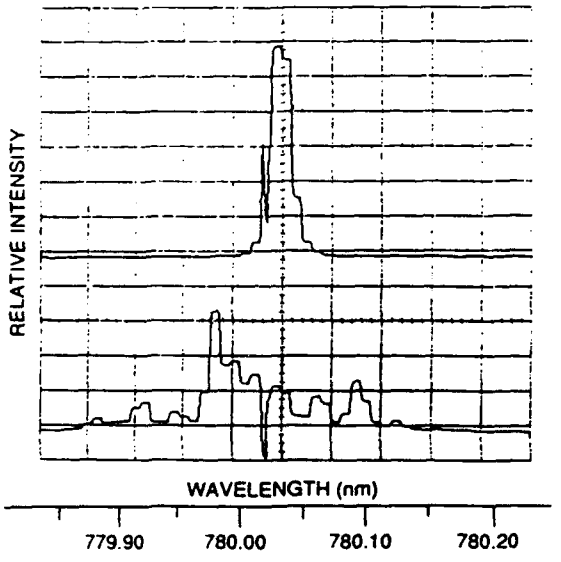

Fig. 2. Oscilloscope traces of Candela LS-1 spectrometer output spectrum. The upper trace shows narrowband operation with injection seeding. The lower trace shows broadband operation with no injection beam. The dip at 780.02 nm is due to a wavelength reference marker. The width of the injection locked trace is due to the resolution of the spectrometer.

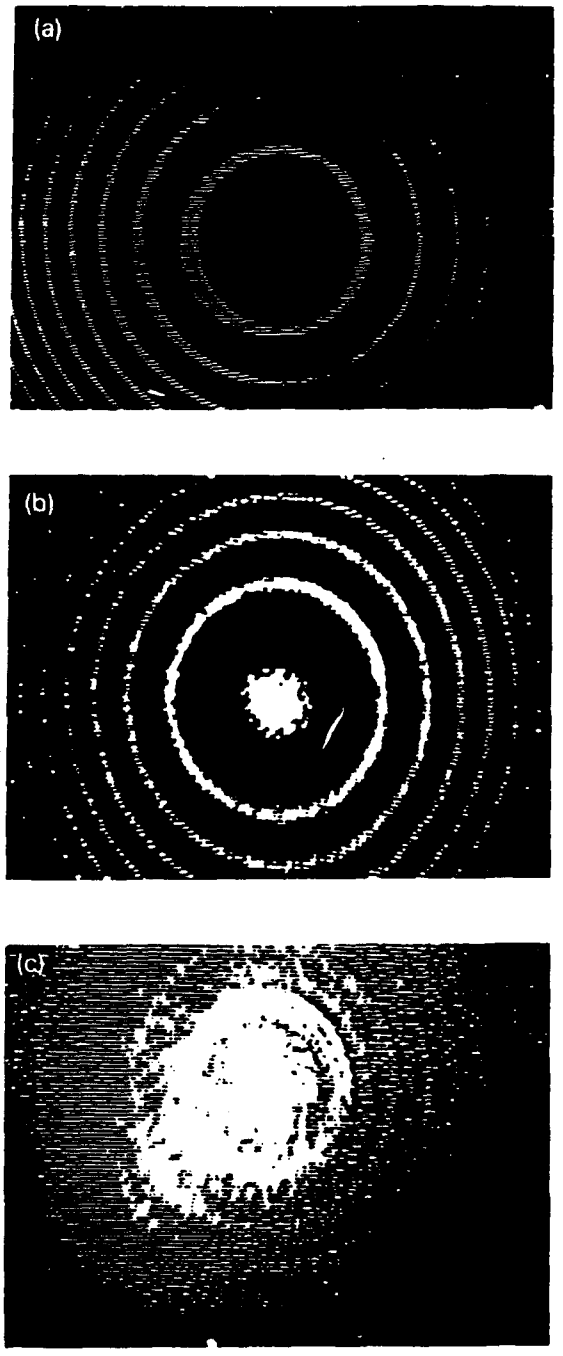

Fig. 3. Single shot Fabry–Pérot interference fringes of (a) the diode laser, (b) the alexandrite laser with injection seeding and (c) the alexandrite laser without injection seeding.

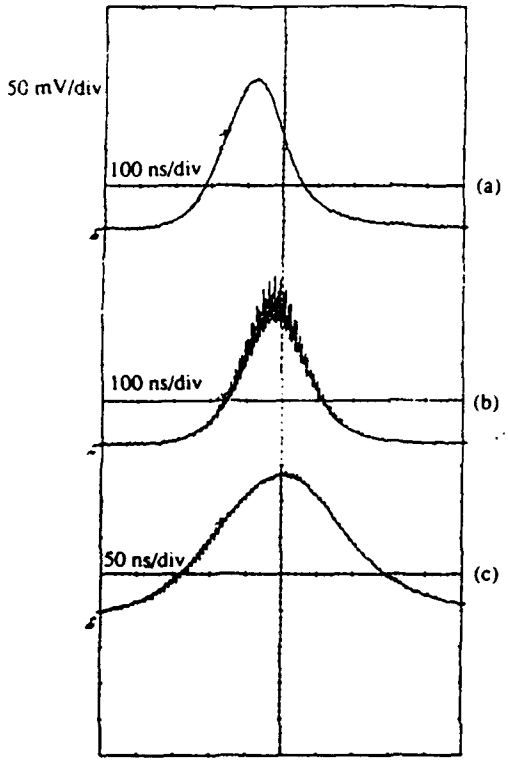

Fig. 4. Q-switched pulse shape. (a) Single longitudinal mode oscillation with injection seeding (194 ns pulse width at fwhm) and (b) multimode (~5 modes) oscillation without injection seeding showing mode beating. (Without injection seeding most of the waveforms look like single mode oscillation since a large number of modes are participating in lasing.) (c) Two mode oscillation with injection seeding showing ~4.3 ns modulation period corresponding to 65 cm cavity length.

ing due to multimode oscillation when the injection seeding is blocked. Without injection seeding most of the output waveforms show a relatively smooth temporal profile since there are many longitudinal modes participating in lasing. Injection seeded waveforms have ~200 ns pulse duration at fwhm and a smooth temporal profile. Occasionally, an injection seeded waveform shows two mode oscillation with a small amplitude modulation of 4.3 ns duration which corresponds to one cavity round trip time (waveform (c)). The modulation depth is very small and it tells us that most of the pulse energy is concentrated in one mode while the other mode shares only a few percent of the total energy in the pulse. While the unseeded beam showed large fluctuations in output power the injection seeded output power remained nearly constant from pulse to pulse.

When the diode laser frequency stabilization circuit was turned off and the diode laser output frequency was tuned slowly, the alexandrite laser output wavelength tracked the change in diode laser frequency over a 20 GHz range which was limited by the laser gain bandwidth restricted by the three plate birefringent filter in the alexandrite laser cavity. With the diode laser locked to the rubidium 5s→5p transition at 780 nm, an experiment was done to look at collisional excitation in a rubidium vapor cell whereby energy pooling led to fluorescence from higher lying levels such as the 6p level (420 nm fluorescence). The amount of fluorescence seen with and without injection seeding is shown in fig. 5. With the laser injection seeded, all of the 780 nm pump

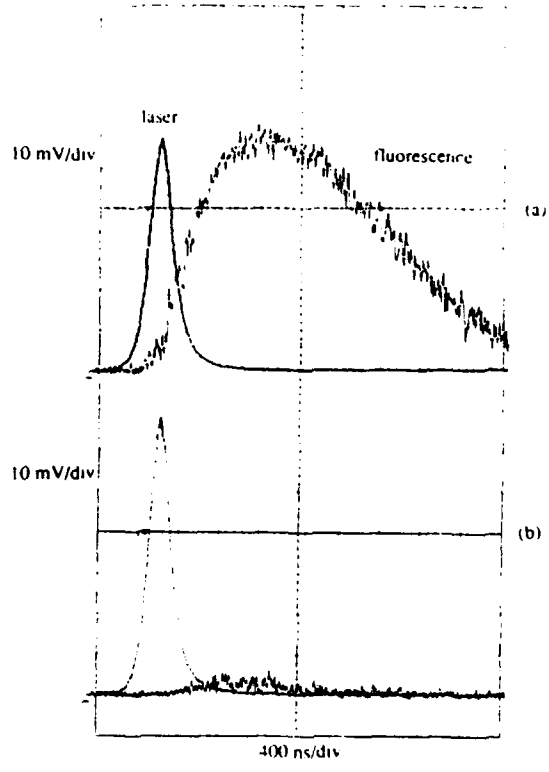

Fig. 5. 420 nm fluorescence generated from a rubidium cell (a) with injection seeded laser beam and (b) with laser beam without injection seeding.

light was absorbed in the cell (6 cm long rubidium cell at 140°C), leading to high excited state densities causing energy pooling. The fluorescence could be seen consistently for many hours while the alexandrite laser was injection seeded, indicating reliable operation.

For good injection seeding several factors such as the spatial overlap of the injection field and the slave oscillator laser field, complete isolation of optical feedback from the slave oscillator to the diode laser and removal of residual birefringence due to the misalignment of the laser rod and Q-switch have to be dealt with. We were able to mode match the diode laser beam to the alexandrite laser by adjusting the diode laser beam collimating lens in the diode laser head. The complete removal of optical feedback into the diode laser was a technical challenge. Optical feedback induced random frequency fluctuations in the diode laser output made the cavity locking very difficult.

5. Conclusion

We were able to demonstrate injection seeding of an alexandrite laser by a diode laser whose frequency was locked to an atomic absorption line of rubidium. As a result of this we were able to get injection seeded output pulses of 10 mJ per pulse energy at 780 nm with ~200 ns fwhm pulse duration and 3 Hz pulse repetition rate. By using the side injection technique high efficiency injection seeding was obtained with small injection power. This system showed excellent long term stability and day-to-day reliability.

Acknowledgements

This research was supported by ONR/SDIO under contract N00014-89-C-0068. The authors would like to thank Dr. K. Wu, Mr. G. Beaghler and Dr. V. Smiley for their encouragement and support.

References

[1] E. Korevaar, M. Rivers and C.S. Liu, SPIE Vol. 1059 Space sensing communications, and networking (1989) p. 111.
[2] C.D. Nabors, A.D. Farinas, T. Day, S.T. Yang, E.K. Gustafson and R.L. Byer, Optics Lett. 14 (1989) 1189.
[3] W.R. Rapoport, J.J. Yeh and R.C. Sam, CLEA '83 Technical Digest (1983) 206.
[4] J. Krasinski, P. Papanestor, J.A. Pete and D.F. Heller, Tunable solid state lasers II (Springer, Berlin, 1988) p. 191.
[5] Y.K. Park, G. Giuliani and R.L. Byer, IEEE J. Quantum Electron. QE-20 (1984) 117.
[6] J.S. Krasinski, Y.B. Band, T. Chin, D.F. Heller, R.C. Morris and P.A. Papanestor, Optics Lett. 14 (1989) 393.
[7] S.W. Henderson, E.H. Yuen and E.S. Fry, Optics Lett. 11 (1986) 715.

5. Combat ID

COMBAT IDENTIFICATION USING A FARADAY FILTER

J. Menders and P. Searcy

ABSTRACT

This project produced a preliminary demonstration of an optical combat identification (CID) system featuring an optical receiver with an atomic line filter. These filters are needed for optical receivers to detect weak signals at the quantum limit in the presence of background noise. Without adequate background rejection, compensating increases in laser power are required. We designed and constructed a CID system comprised of a low power, (ANSII standard) eyesafe diode laser interrogator, a modulated retro-reflector responder and an optical receiver with an atomic line filter. To permit hand pointing of the interrogator, the interrogator beam divergence and receiver field of view were large, > 1 mrad. The system was designed to show that a responder identification code could be read at a range of about 5 km. Preliminary tests at 0.25 km demonstrated code reception by the filtered receiver.

INTRODUCTION

Our matched ultra-narrowband transceiver approach to optical CID uniquely features atomic line filter (Faraday filter) technology; however, our overall approach to optical CID is generic. Our overall approach consists of equipping friendly platforms with passive responders which impress an identifying code on an interrogation beam originating from a weapons platform. Here, the optical responders are retroreflectors with a liquid crystal modulator. In general, the range required for a system must match that of the associated weapon. Similarly, the interrogator pointing tolerance should be equal to or greater than that of the weapon.

Additional design complexity is driven by other system and component requirements. The system design must consider the need to conceal the responder from enemy sensors. The common approach to concealing the responder is for its aperture to remain normally closed until a "wake-up" signal is received, initiating a response. However, because of scarce

resources, we limited our development to the interrogator, comprised of the laser and the receiver, and the responder.

Our primary goal in the development of this hardware was to produce a CID demonstrator ready for field demonstrations at a range of about 5 km. The system would be eyesafe, portable and easy to operate. We completed this program with mixed results. We did demonstrate responder code interrogation using a Faraday filtered receiver at a range of about 0.25 km, as described below. The demonstration utilized a frequency matched single mode diode laser, a liquid crystal modulated responder operating in the field at 10 kHz and a Faraday filtered receiver. Because we did not yet possess a laser ready for out-of-doors operation, we set the interrogator up inside our building, and linked with a responder at the longest possible distance outside. We observed the responder signal and signal power measurements confirmed our link budget analysis. However, the test also revealed a serious shortcoming in our custom integrated detector/high gain current preamplifier: the dynamic range was not sufficient to accomodate the moderate amplitude fluctuations present in the scintillated responder signal.

Solutions to these difficulties are now at hand. We have just completed a small production run of a locked diode laser, ruggedized for an aircraft application, which can be operated out-of-doors. In addition, since the conclusion of the effort, we have obtained and tested new, off-the-shelf detector/preamplifiers with the required gain, noise and dynamic range characteristics. We describe the new diode laser and detector/preamplifier performance in the field test equipment descriptions below.

SYSTEM DESCRIPTION

A block diagram of the system is shown in Fig. 1. The interrogator, on the left hand side of the figure, consists of the optical head, driver electronics and signal processor. The optical head consists of a locked laser transmitter, a filtered optical receiver and a sight. The locked transmitter is a single mode diode laser at about 852 nm, precisely tuned to the 6 GHz passband of the Faraday filter passband in the receiver. The beam divergence of >1 mrad is wide enough to make illumination of the responder possible using the sight. The

beam is impressed with a 16 bit modulation (identification code) at 10 kHz and retro-reflected by the responder. The receiver collects the signal, and passes it through the Faraday filter to a combination avalanche photodiode and preamplifier. The signal is digitized and processed to retrieve the identification code.

To avoid drop out in signal transmission by atmospheric scintillation, the modulation rate of the system was chosen such that an identification code could be transmitted within the scintillation period of about 1 ms. Thus, a modulation rate of >10 kHz is required for a 10 bit code. Fortunately, a modulation rate of about 10 kHz can be provided by a ferro-electric liquid crystal, a potentially low cost device.

A link calculation of the total signal power incident on the photodetector as a function of range shown in Fig. 2, was developed to assess the range capability of the system. The calculation assumes that the interrogator transmits about 150 mW in a 1 mrad divergent beam, a 25 mm responder aperture, a 45 mm receiver aperture and appropriate optical attenuation coefficients. The calculation neglects atmospheric scintillation. The estimate predicts a responder signal of about 100 pW at the 5 km range goal.

LASER TRANSMITTER

For the demonstration described below, the laser transmitter consisted of a 150 mW diode laser tuned to the passband of the Faraday filter. We used a Spectra Diode Labs model SDL-5420 with a room temperature wavelength of 852 nm, which could be temperature/current tuned to the filter passband. The diode was mounted in a temperature controlled mount, and driven using a precision low noise current supply. Because the tuning of this laser was sensitive to ambient small temperature variations brought about by exposure to drafts, it was necessary to operate this laser in the conditioned environment of our building. In addition, this laser was susceptible to frequency drift with current drift and destabilization by feedback typically originating from local beam steering optics.

ThermoTrex now produces a temperature and feedback resistant feedback locked diode laser, shown in Fig. 3. This 150 mW laser features an external cavity which incorporates

an atomic line filter, fixing the frequency of operation to the filter passband. Laboratory tests have shown that this laser is immune to feedback, and remains frequency locked over large variations in drive current. The enclosure design features an insulating layer designed to provide a stable temperature environment.

RESPONDER

The responder, a modulated retroreflector, is shown in Fig. 4. The retro-reflector is a gold corner cube, with a total beam deviation of 2 arcseconds. Recessed into the retroreflector enclosure is a 1 inch diameter ferro-electric liquid crystal modulator behind a polarcor infrared polarizer. At 852 nm, the liquid crystal can be switched between a zero and quarter waveplate state; in the quarter wave state, the double pass has the effect of rotating the polarization by 90 degrees. The rotated light is then extinguished by the polarizer upon exit.

The one inch responder aperture was the largest off-the-shelf ferro-electric liquid crystal modulator size available. Larger custom made devices were available, but required an unacceptably long lead time.

FARADAY FILTERED RECEIVER

The Faraday filtered receiver is shown in Fig. 5. The entire assembly is portable and battery operated. Light enters the receiver through a bandpass filter and is collected by a fast 2 inch diameter lens. The receiver field-of-view can be varied down to about 1 mrad by a iris at the focal plane of the lens. The signal is then relayed to the 3 mm diameter active area of the avalanche photodiode (APD) by a lens which is integrated into the Faraday filter. The Faraday filter consists of an entrance polarizer followed by a cesium vapor cell in a longitudinal magnetic field and an exit polaizer. The cell is enclosed by windowed air spaces for insulation, the relay lens serving the additional purpose of entry jacket window.

The transmission spectrum of the Faraday filter along with that of a cesium absorption reference cell is shown in Fig. 6. The beam from a frequency ramped diode laser was ramped and passed through the reference cell and Faraday filter simultaneously. The reference cell transmission shows the cesium 6 $^2S_{1/2}$-6 $^2P_{3/2}$ doublet with a spacing of 9.2 GHz. The Faraday filter transmission was designed to provide the relatively wide passband filling the frequency interval between the lines to relax the laser tuning requirements. In this configuration, the filter uses about 1 cm pathlength of vapor at about 100 C in a field of about 100 G. The interrogator emission frequency position is shown.

The APD/preamplifier consisted of a low noise transimpedance amplifier integrated with Hamamatsu photodiode by Analog Modules, Inc. When operated at the recommended gain of M = 60, this APD, model S2384, was characterized by an excess noise factor of 0.3 and a dark noise of 1 nA. For a beam divergence of 5 mrad, the signal light at about 100 pW was expected to dominate the background light. Then, noise equivalent power including the shot noise and the excess noise (but ignoring the preamplifier noise) was estimated to be about 1 pW, giving a signal to noise ratio of 100. However, at these levels, the preamplifier would be the dominant noise source. To minimize the noise, amplifier gain bandwidth was set to about 25 kHz. Furthermore, by setting the amplifier cut-on to about 1 kHz, we attempted remove the 1/f noise at low frequencies and to block low frequency atmospheric scintillation noise. Analog Modules delivered an integrated APD/preamplifier with a transimpedance gain of 10 MΩ and a noise density of 550 fA/$\sqrt{\text{Hz}}$, corresponding to a contribution of about 2 pW. However, as we learned durnig our tests, the small dynamic range of the APD/preamplifier limited its application to short ranges. In the lab we tested the receiver response against the amplitude of an optical square wave input. We found that the receiver exhibited a threshold and a saturation level that was only 3 times threshold!

We have since received an off-the-shelf APD/preamplifier, the Advanced Photonics APM-22, that should enable 3 km interrogations. This unit features a 5 mm active area, gain from DC to 35 kHz and a transimpedance gain of 1 MΩ. In laboratory evaluations, we measured the noise density of the ADP/preamplifier at M=50 under 100 pW illumination at 633 nm to be about 1 pW/rt Hz. Thus, at the receiver bandwidth of 20 kHz, we expect an

NEP of about 150 pW, giving a signal to noise ratio of about 10 at a range of 3 km. In addition, we have observed linear response of photoreceiver from 1 pW to >1 μW.

DEMONSTRATION EXPERIMENT

We performed field test to demonstrating responder interrogation at a range of 0.25 km. This demonstration included the laser transmitter, responder and receiver described in the paragraphs above. Fig. 7 shows the interrogator and the responder during the test. Because the frequency locked laser was not yet operable out-of-doors, we used a diode laser in a standard mount, tuned to the Faraday filter passband. The photograph of the interrogator shows a short optical rail, mounted on a tripod, supporting the laser on the right and the receiver on the left. A sighting scope is built into the center of the rail. Because the retroreflected beam was only inches in extent, it was necessary to launch the interrogator beam from a position in front of the receiver. In addition, rapid alignment was facilitated using a camera to observe the beam striking on the target.

The laser transmitter beam was about 125 mW, with a divergence of about 1 mrad. Once the sighting scope was co-aligned, it could be used to illuminate the responder. The responder was positioned at range and set up to provide a repetitve 16 bit sequence at about 10 kHz. The sequence consisted of a "start character" consisting of 4 off bits, several alternating bits and a "stop character" consisting of 2 on bits. The return beam was received and captured using a digital oscilloscope. Fig. 8 shows responder signals at 30 and 260 m range. The signal at close range shows a cleanly received signal. An extended measurement of the long range signal (Fig. 7b) over 100 ms shows how atmospheric scintillation corrupted the signal detected by our dynamic range limited receiver. The figure detail of the long range signal (Fig. 7c) shows how the receiver threshold and saturation behavior limits receiver response to a narrow range of signal amplitudes.

RECOMMENDATIONS FOR FURTHER DEVELOPMENT

The results of this program indicate that this combat identification scheme could demonstrate responder interrogation in the field with augmentation. We can now provide a

new, ruggedized frequency locked diode laser suitable for field operation. In recent months, new off the shelf photo-receivers have become available with the required performance. These enhancements should provide responder interrogation at a range of 3 km. Additional range can be obtained by increasing the area of the responder. If the return beam spot size is proportional to the diffraction limit, then the signal received is proportional to the respnder diameter D^4, and inversely proportional to the range R^4. Thus, the two inch diameter responder, obtainable as a custom product, could extend the range to 6 km.

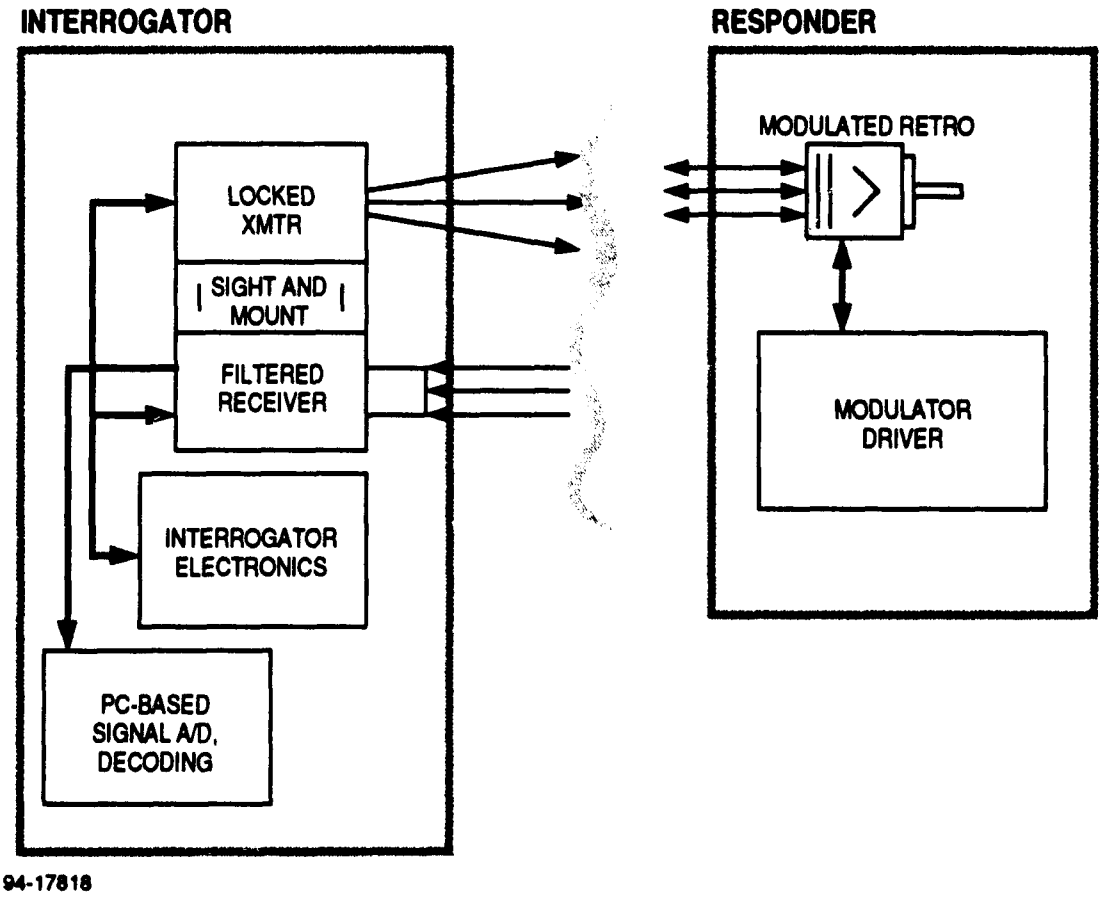

Figure 1. Combat ID system block diagram.

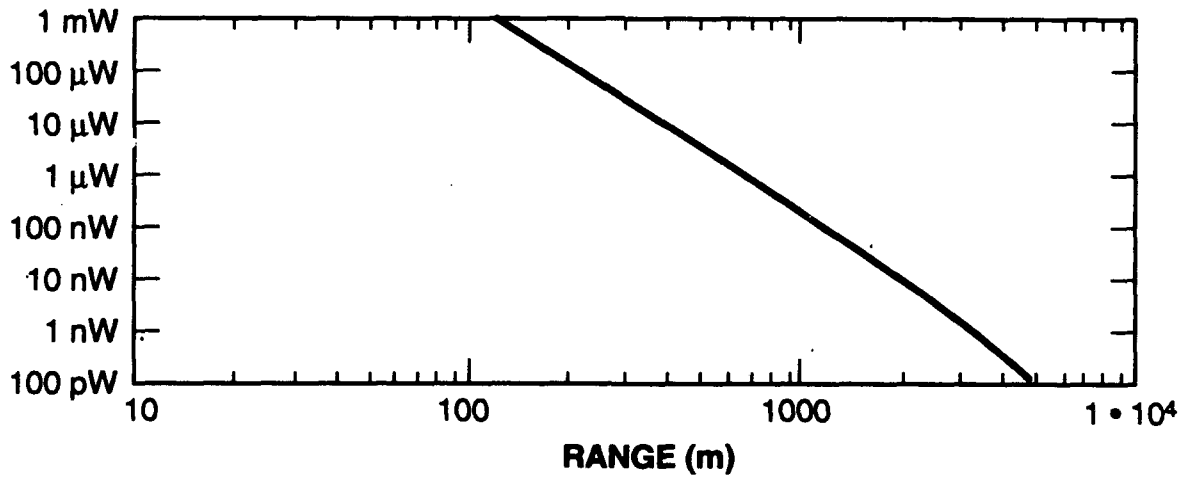

94-17817

Figure 2. Signal power incident on the photodetector as a funtion of range.

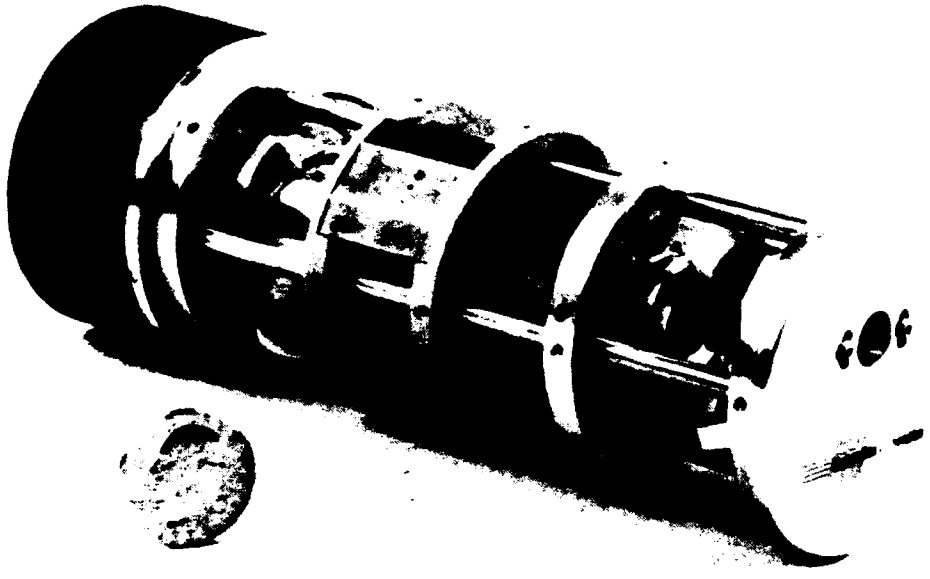

93-16519a

Figure 3. TTC frequency locked diode laser.

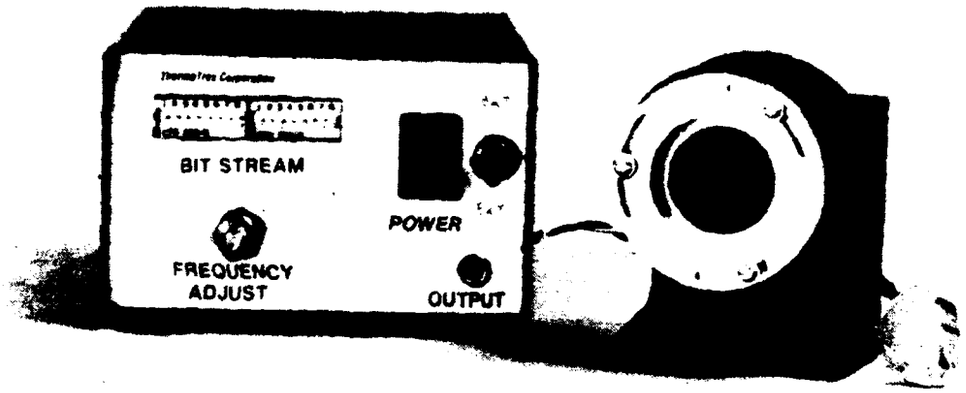

94-17816

Figure 4. The responder consists of a moduled retro-reflector and driver.

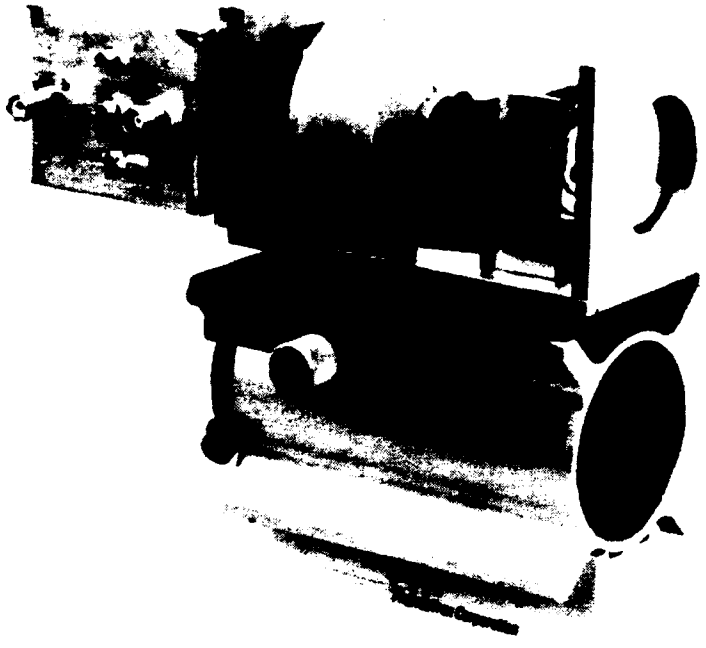

94-17815

Figure 5. Interrogator receiver with Faraday filter.

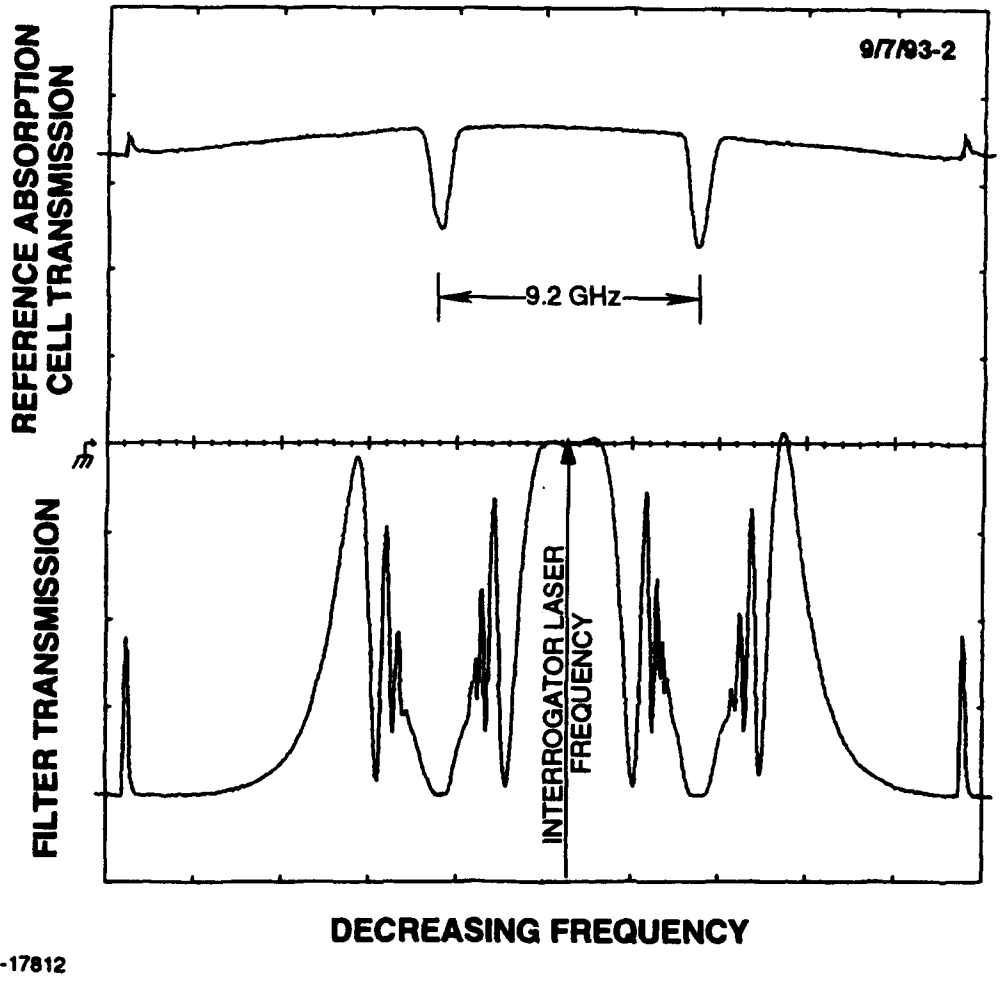

Figure 6. Receiver filter transmission spectrum.

94-17813

Figure 7. Interrogator (right) and responder set-up (left) during field tests.

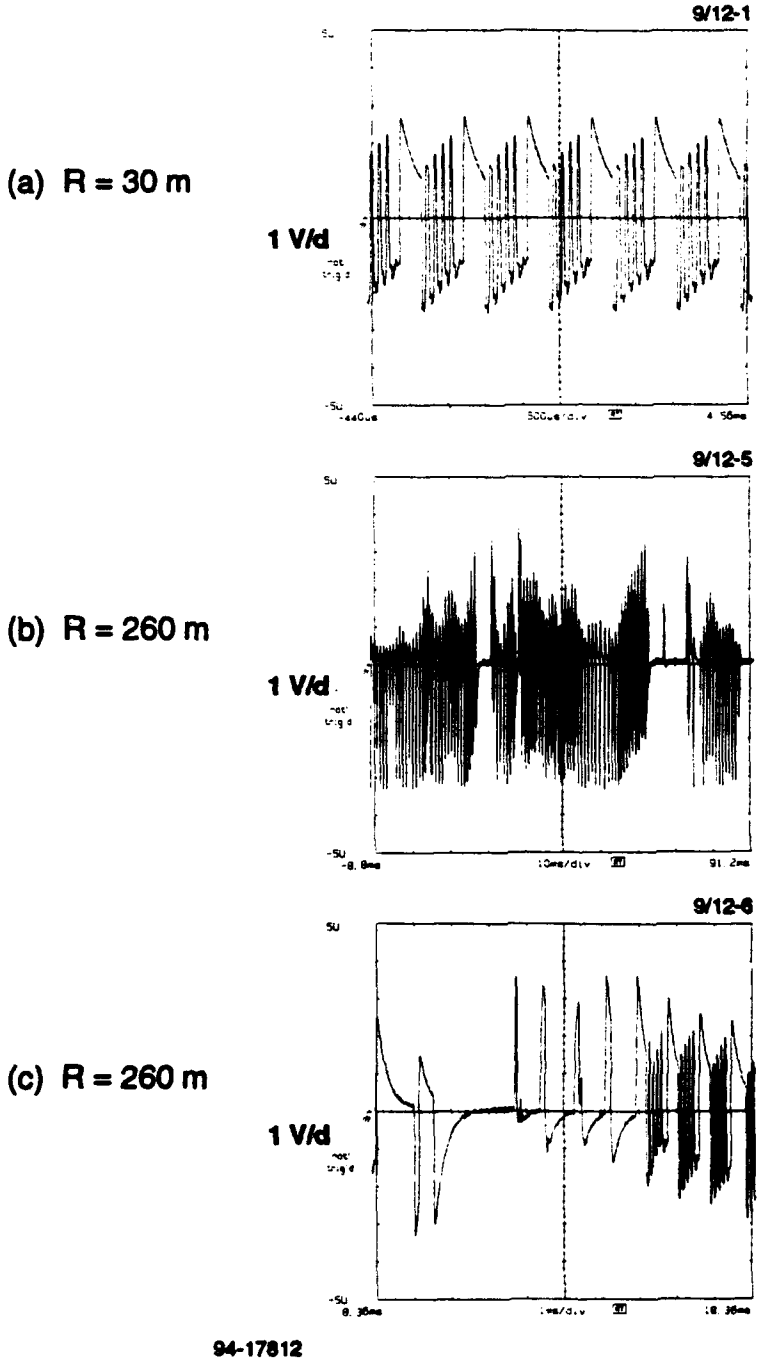

Figure 8. Responder signals detected by atomic line filtered receiver.